METEOROLOGISKA INSTITUTIONEN
vid
KUNGL. UNIVERSITETET
UPPSALA

LEIF ENGER

NUMERICAL BOUNDARY LAYER MODELING WITH APPLICATION TO DIFFUSION

PART I

A TWO DIMENSIONAL HIGHER ORDER CLOSURE MODEL

REPORT NO. 70

UPPSALA 1983

LEIF ENGER

NUMERICAL BOUNDARY LAYER MODELING WITH APPLICATION TO DIFFUSION

PART I

A TWO DIMENSIONAL HIGHER ORDER CLOSURE MODEL

REPORT NO. 70

UPPSALA 1983

UNIV.
LEIDEN
BIBL.

Doctoral Thesis at the University of Uppsala 1983

ABSTRACT

Enger, L., 1983. Numerical boundary layer modeling with application to diffusion. Part I: A two dimensional higher order closure model. *Department of Meteorology, University of Uppsala. Report No 70.* 54 pp, ISBN 91-506-0385-X.

A two-dimensional second-order closure model based on the so called Level 3 model of Mellor and Yamada (1974) is presented. Recent atmospheric and laboratory data are used to set up sophisticated and realistic formulations of the turbulent length scales. The result of this is shown to be a clear improvement compared to the original model version of Mellor and Yamada. Tests, regarding the mean quantities, have been done with a one-dimensional version of the model on Wangara data. The turbulent quantities in a convective boundary layer have been tested against laboratory data as well as other field data and simulations with other higher-order closure models. A two-dimensional version is tested against wind data from a field experiment in the island of Gotland in the Baltic (Faxén, 1980).

The model seems to simulate fairly well both the mean quantities and the turbulent quantities, expressed in the framework of the convective similarity theory if proper values of the proportionality factors for the turbulent length scales are used. The simulations of the Gotland data show reasonable agreement, which is encouraging in view of the fact that the experimental situation was far from ideally two-dimensional.

Leif Enger, Department of Meteorology, University of Uppsala, Box 516, S-751 20 Uppsala, Sweden.

ISBN 91-506-0385-X

© Leif Enger
Printed in Sweden by
Department of Meteorology
Uppsala University, 1983

CONTENTS

		page
	ABSTRACT	2
1	INTRODUCTION	4
2	DESCRIPTION OF THE MODEL	6
2.1	*Governing equations*	6
2.2	*The turbulent length scale*	11
	Neutral condition. Surface layer	11
	Unstable condition. Surface layer	11
	Stable condition. Surface layer	13
	Unstable condition. Transition layer	16
	Stable condition. Transition layer	17
	Near neutral condition	18
2.3	*The model coefficients*	18
2.4	*Boundary conditions*	21
2.5	*Initial conditions*	23
2.6	*The geostrophic wind*	23
2.7	*The grid system and the finite-difference scheme*	23
3	TESTS	26
3.1	*Mean temperature, heat flux and temperature fluctuations*	26
3.2	*Mean wind and velocity fluctuations*	27
3.3	*Height of the mixed layer*	29
3.4	*Sensitivity tests*	29
3.5	*Test of the two-dimensional version of the model*	30
	SUMMARY AND CONCLUSIONS	36
	ACKNOWLEDGEMENTS	37
	REFERENCES	38
	FIGURES	41

1 INTRODUCTION

During the last two decades our knowledge of the planetary boundary layer has improved considerably. This is partly due to a number of well planned and successful field experiments: the Kansas experiment (Haugen et al., 1971), the Wangara experiment (Clarke et al., 1971) and the Minnesota experiment (e.g., Kaimal et al., 1976) just to mention a few. But there has also been considerable success in numerical modelling from the early attempts by Estoque (1963) to the very complex model by Deardorff (1974).

The principal difficulty in the modelling of the planetary boundary layer is the so called closure problem. This problem arises as a result of the averaging process which is necessary in all numerical treatment of turbulent flows because of the enormous range of length scales present. Thus, averaging of the equation of motion generates a number of second order moments, the nine components of the tensor $\overline{u_i u_j}$. If there is buoyancy in the flow there are another three terms, $\overline{u_i \theta}$. Classical K-theory is the simplest way to deal with this problem. It is in essence an analogy to molecular diffusion and thus postulates the various moments, interpreted as fluxes, to be proportional to the local gradients of the corresponding mean fields. This approach can be proved (e.g. Tennekes and Lumley, 1972) to be incorrect in general, but correct in certain special cases – one important case being the atmospheric surface layer.

It is, however, possible to write down formal balance equations for all the second order moments. But these equations contain a great number of third order moments, i.e. $\overline{u_i u_j u_k}$, $\overline{u_i p}$ etc. Balance equations can be written for everyone of these, but this generates a still larger amount of fourth order moments etc ad infinitum.

Second order closure modelling means carrying out the equations for the mean flow, which contains the second order moments, and in addition also carrying out the balance for these moments but parameterizing the third order moments.

Second order models can be of varying complexity depending on which closures are being made. Mellor and Yamada (1974) introduce another nomenclature for first and second order models, Level 1 to Level 4, where the Level 4 model is the most complex one, involving 10 differential equations for the second order moments. In the Level 3 model simplifications are made by relative ordering of all terms. They end up with two differential equations and eight algebraic equations for the second order moments. Levels 1 and 2 are further simplified ones

Digitized by the Internet Archive
in 2026

https://archive.org/details/IA41549218_0010

which involve only algebraic equations for the second order moments and are therefore of the first order type models. Mellor and Yamada (1974) also show that the Level 4 model gives very little extra information compared with a Level 3 model, but a Level 4 model is much more computer time consuming as one has to solve ten differential equations for the second order moments instead of two in a Level 3 model.

At the Meteorological Department in Uppsala we are in the process of building up a model which can be used for various applications such as dispersion calculations and wind energy prospecting. The model has to be so complex that it gives information about the turbulent quantities but at the same time to simple that it is not too computer time consuming. We have therefore chosen to use a Level 3 model.

In the present paper a first version of this model is presented. In this version the following assumptions and simplifications are made:

1) The model is two-dimensional.
2) The equation for water vapor is excluded.
3) The flux divergence of radiation is excluded.
4) The equation for the energy balance at the surface is excluded; instead we give the temperature at screen level.

The one-dimensional version of this model is tested against:

1) Atmospheric experiment data, Wangara data DAY33-DAY35, for the mean variables (Clarke et al., 1971).
2) Water tank experiment (Willis and Deardorff, 1974).
3) Other numerical models (Deardorff (1974), André et al., (1976) and Wyngaard and Coté (1974)) for the turbulent quantities.

The two-dimensional version is tested against data from measurements in the island of Gotland, Sweden (Faxén, 1980).

2 DESCRIPTION OF THE MODEL

The present model deals onoy with clear boundary layers, i.e. with situations where the humidity is low enough to avoid condensation. Another report (Grandin, 1983) deals with the condensation processes in the atmosphere and in a later stage we will couple these two models together. We shall further assume that the PBL is homogeneous in the y-direction, meaning for example that we can study problems concerning interaction between the atmosphere over land and sea in cases with a straight coast line. The meteorological variables we shall consider are the velocity components U (x-direction), V (y-direction) and W (z-direction) and the potential temperature. The mixing ratio of water vapor is excluded from our set of equations in the present model version.

2.1 *Governing equations*

The present model is based on Mellor's and Yamada's Level 3 model (Mellor and Yamada, 1974 and Yamada and Mellor, 1975). A Level 3 model requires solution of only two out of ten differential equations that constitute the more complete Level 4 type of models, namely the equations for the turbulent kinetic energy and for the temperature variance.

The equations of motion for the mean velocity and mean virtual potential temperature for the two dimensional case are

$$\frac{\partial U}{\partial t} + U\frac{\partial U}{\partial x} + W\frac{\partial U}{\partial z} - f\,V + f\,V_g = \frac{\partial}{\partial x}\left(-\overline{u^2}\right) + \frac{\partial}{\partial z}\left(-\overline{uw}\right) \tag{1}$$

$$\frac{\partial V}{\partial t} + U\frac{\partial V}{\partial x} + W\frac{\partial V}{\partial z} + f\,U - f\,U_g = \frac{\partial}{\partial x}\left(-\overline{uv}\right) + \frac{\partial}{\partial z}\left(-\overline{vw}\right) \tag{2}$$

$$\frac{\partial U}{\partial x} + \frac{\partial W}{\partial z} = 0 \tag{3}$$

$$\frac{\partial \Theta}{\partial t} + U\frac{\partial \Theta}{\partial x} + V\frac{\partial \Theta}{\partial y} + W\frac{\partial \Theta}{\partial z} = \frac{\partial}{\partial x}\left(-\overline{u\theta}\right) + \frac{\partial}{\partial z}\left(-\overline{w\theta}\right) + \sigma_r \tag{4}$$

where U, V, W, Θ are the mean velocities in the x-, y-, z-directions and virtual potential temperature, respectively. f is the Coriolis parameter, $\overline{u^2}$, $\overline{uw}$, $\overline{uv}$ and $\overline{vw}$ are components of the Reynold's stress tensor, $\overline{u\theta}$ and $\overline{w\theta}$ are components of the kinematic turbulent heat flux and σ_r is the flux divergence of radiation. U_g and V_g are the geostrofic wind components in x- and y-direction respectively.

The Level 3 model requires solution of two more differential equations, namely for q^2 and $\overline{\theta^2}$, where q^2 is twice the turbulent energy and $\overline{\theta^2}$ is the temperature variance. In the two dimensional version using Yamada's and Mellor's closure hupothesis these are

$$\frac{\partial q^2}{\partial t} + U\frac{\partial q^2}{\partial x} + W\frac{\partial q^2}{\partial z} - \frac{\partial}{\partial x}\left(\frac{5}{3}q\lambda_1\frac{\partial q^2}{\partial x}\right) - \frac{\partial}{\partial z}\left(\frac{5}{3}q\lambda_1\frac{\partial q^2}{\partial z}\right) =$$

$$= -2\overline{u^2}\frac{\partial U}{\partial x} - 2\overline{uw}\frac{\partial U}{\partial z} - 2\overline{uv}\frac{\partial V}{\partial x} - 2\overline{vw}\frac{\partial V}{\partial z} - 2\overline{uw}\frac{\partial W}{\partial x} - 2\overline{w^2}\frac{\partial W}{\partial z} +$$

$$+ 2\beta g\,\overline{w\theta} - 2\frac{q^3}{\Lambda_1} \qquad (5)$$

$$\frac{\partial\overline{\theta^2}}{\partial t} + U\frac{\partial\overline{\theta^2}}{\partial x} + W\frac{\partial\overline{\theta^2}}{\partial z} - \frac{\partial}{\partial x}\left(q\lambda_2\frac{\partial\overline{\theta^2}}{\partial x}\right) - \frac{\partial}{\partial z}\left(q\lambda_2\frac{\partial\overline{\theta^2}}{\partial z}\right) - 2\overline{u\theta}\frac{\partial\Theta}{\partial x} -$$

$$- 2\overline{w\theta}\frac{\partial\Theta}{\partial z} - 2\frac{q}{\Lambda_2}\overline{\theta^2} \qquad (6)$$

where λ_1, λ_2, Λ_1 and Λ_2 are turbulent length scales which are supposed to be proportional to each other and β is the coefficient of thermal expansion.

As shown in Yamada and Mellor (1974), once $\overline{q^2}$ and $\overline{\theta^2}$ have been obtained, the components of Reynold's stress and heat flux can be expressed by analytical expressions. If we make use of the continuity equation, Eq (3), these analytical expressions take the following forms in the two-dimensional case:

$$\overline{u^2} = \frac{1}{1+\frac{4\ell_1}{q}\frac{\partial U}{\partial x}}\left\{\frac{q^2}{3} + \frac{\ell_1}{q}\left[-4\overline{uw}\frac{\partial U}{\partial z} + 2\overline{vw}\frac{\partial V}{\partial z} - \left(2\overline{w^2} - 6cq^2\right)\frac{\partial U}{\partial x} +\right.\right.$$

$$\left.\left. + 2\overline{uv}\frac{\partial V}{\partial x} + 2\overline{uw}\frac{\partial W}{\partial x} - 2\beta g\,\overline{w\theta}\right]\right\} \qquad (7a)$$

$$\overline{v^2} = \frac{q^2}{3} + \frac{\ell_1}{q}\left[2\overline{uw}\frac{\partial U}{\partial z} - 4\overline{vw}\frac{\partial V}{\partial z} + 2\left(\overline{u^2} - \overline{w^2}\right)\frac{\partial U}{\partial x} - 4\overline{uv}\frac{\partial V}{\partial x} +\right.$$

$$\left. + 2\overline{uw}\frac{\partial W}{\partial x} - 2\beta g\,\overline{w\theta}\right] \qquad (7b)$$

$$\overline{w^2} = \frac{1}{1 - \frac{4\ell_1}{q}\frac{\partial U}{\partial x}} \left\{ \frac{q^2}{3} + \frac{\ell_1}{q} \left[2\,\overline{uw}\,\frac{\partial U}{\partial z} + 2\,\overline{vw}\,\frac{\partial V}{\partial z} - 4\,\overline{uw}\,\frac{\partial W}{\partial x} + \right.\right.$$

$$\left.\left. + \left(2\overline{u^2} - 6c\overline{q^2}\right)\frac{\partial U}{\partial x} + 2\overline{uv}\,\frac{\partial V}{\partial x} + 4\,\beta g\,\overline{w\theta} \right] \right\} \qquad (7c)$$

$$-\overline{uv} = \frac{1}{\frac{q}{3\ell_1} + \frac{\partial U}{\partial x}} \left\{ \overline{uw}\,\frac{\partial V}{\partial z} + \overline{vw}\,\frac{\partial U}{\partial z} + \left(\overline{u^2} - c\,q^2\right)\frac{\partial V}{\partial x} \right\} \qquad (8a)$$

$$-\overline{uw} = \frac{3\ell_1}{q} \left\{ \left(\overline{w^2} - c\,q^2\right)\frac{\partial U}{\partial z} + \left(\overline{u^2} - cq^2\right)\frac{\partial W}{\partial x} - \beta g\,\overline{u\theta} \right\} \qquad (8b)$$

$$-\overline{vw} = \frac{1}{\frac{q}{3\ell_1} - \frac{\partial U}{\partial x}} \left\{ \left(\overline{w^2} - c\,q^2\right)\frac{\partial V}{\partial z} + \overline{uw}\,\frac{\partial V}{\partial x} + \overline{uv}\,\frac{\partial W}{\partial x} - \beta g\,\overline{v\theta} \right\} \qquad (8c)$$

$$-\overline{u\theta} = \frac{1}{\frac{q}{3\ell_2} + \frac{\partial U}{\partial x}} \left\{ \overline{u^2}\,\frac{\partial \Theta}{\partial x} + \overline{uw}\,\frac{\partial \Theta}{\partial z} + \overline{w\theta}\,\frac{\partial U}{\partial z} \right\} \qquad (9a)$$

$$-\overline{v\theta} = \frac{3\ell_2}{q} \left\{ \overline{uv}\,\frac{\partial \Theta}{\partial x} + \overline{vw}\,\frac{\partial \Theta}{\partial z} + \overline{w\theta}\,\frac{\partial V}{\partial z} + \overline{u\theta}\,\frac{\partial V}{\partial x} \right\} \qquad (9b)$$

$$-\overline{w\theta} = \frac{1}{\frac{q}{3\ell_2} - \frac{\partial U}{\partial x}} \left\{ \overline{uw}\,\frac{\partial \Theta}{\partial x} + \overline{w^2}\,\frac{\partial \Theta}{\partial z} + \overline{u\theta}\,\frac{\partial W}{\partial x} - \beta g\,\overline{\theta^2} \right\} \qquad (9c)$$

ℓ_1 and ℓ_2 are turbulent length scales supposed to be proportional to each other so $\ell_1 = A_1\ell$ and $\ell_2 = A_2\ell$. c is a constant.

The calculation of the vertical turbulent fluxes of momentum, $\rho\,\overline{uw}$ and $\rho\,\overline{vw}$, and of the virtual potential temperature, $\overline{w\theta}$, can be simplified further. After some algebraic manipulation with equations (7) - (9) we get:

$$-\overline{uw} = K_M\,\frac{\partial U}{\partial z} + \gamma_a \qquad (10a)$$

$$-\overline{vw} = K_M\,\frac{\partial V}{\partial z} + \gamma_b \qquad (10b)$$

$$-\overline{w\theta} = K_H\,\frac{\partial \Theta}{\partial z} - \gamma_c \qquad (11)$$

where

$$K_M = A_1 \ell \left\{ \left(\frac{1}{1 - \frac{4A_1 \ell}{q} \frac{\partial U}{\partial x}} - 3c \right) q^5 - \frac{9\beta g A_2 \ell^2 (4A_1 c + A_2)}{\left(1 - \frac{3A_2 \ell}{q} \frac{\partial U}{\partial x}\right)\left(1 - \frac{4A_1 \ell}{q} \frac{\partial U}{\partial x}\right)} \frac{\partial \Theta}{\partial z} q^3 + \right.$$

$$+ 9(\beta g)^2 q A_2 \ell^2 \frac{1}{1 - \frac{3A_2 \ell}{q} \frac{\partial U}{\partial x}} \left(\frac{4A_1}{1 - \frac{4A_1 \ell}{q} \frac{\partial U}{\partial x}} + 3A_2 \right) \overline{\theta^2} + 3A_1 \ell \times$$

$$\times \left(q^2 - \frac{9A_2^2 \ell^2 \beta g}{1 - \frac{3A_2 \ell}{q} \frac{\partial U}{\partial x}} \frac{\partial \Theta}{\partial z} \right) \frac{1}{1 - \frac{4A_1 \ell}{q} \frac{\partial U}{\partial x}} \left[-4\overline{uw} \frac{\partial W}{\partial x} + \left(2u^2 - 6cq^2\right) \frac{\partial U}{\partial x} + 2\overline{uv} \frac{\partial V}{\partial x} \right] -$$

$$\left. - 9\beta g A_2 \ell^2 q \frac{1}{1 - \frac{3A_2 \ell}{q} \frac{\partial U}{\partial x}} \left(\frac{4A_1}{1 - \frac{4A_1 \ell}{q} \frac{\partial U}{\partial x}} + 3A_2 \right) \times \left(\overline{uw} \frac{\partial \Theta}{\partial x} + \overline{u\theta} \frac{\partial W}{\partial x} \right) \right\} / M \qquad (12a)$$

$$K_H = \frac{A_2 \ell}{\left(1 - \frac{4A_1 \ell}{q} \frac{\partial U}{\partial x}\right)} \left\{ q^3 + 6A_1 \ell \left(\overline{uw} \frac{\partial U}{\partial z} + \overline{vw} \frac{\partial V}{\partial z} \right) - 12A_1 \ell \, \overline{uw} \frac{\partial W}{\partial x} + \right.$$

$$\left. + 6A_1 \ell \left[\left(\overline{u^2} - 3cq^2 \right) \frac{\partial U}{\partial x} + \overline{uv} \frac{\partial V}{\partial x} \right] \right\} / N \qquad (12b)$$

$$\gamma_a = q^4 \frac{R P \left(\frac{M}{q^4} - Q \left(\frac{\partial U}{\partial z} \right)^2 \right) - S P Q \frac{\partial U}{\partial z} \frac{\partial V}{\partial z}}{M \left(\frac{M}{q^4} - Q \left| \frac{\partial V}{\partial z} \right|^2 \right)} \qquad (13a)$$

$$\gamma_b = q^4 \frac{S P \left(\frac{M}{q^4} - Q \left(\frac{\partial V}{\partial z} \right)^2 \right) - S P Q \frac{\partial U}{\partial z} \frac{\partial V}{\partial z}}{M \left(\frac{M}{q^4} - Q \left| \frac{\partial V}{\partial z} \right|^2 \right)} \qquad (13b)$$

$$\gamma_c = 3A_2 \ell q \frac{\beta g \overline{\theta^2} - \overline{uw}\frac{\partial \Theta}{\partial x} - \overline{u\theta}\frac{\partial W}{\partial x}}{N} \tag{13c}$$

$$K_M = q^4 + 6A_1^2 \ell^2 q^2 \frac{1}{1 - \frac{4A_1 \ell}{q}\frac{\partial U}{\partial x}} \left|\frac{\partial \mathbb{V}}{\partial z}\right|^2 + 3A_1 A_2 \ell^2 \left\{ \frac{4q^2}{\left(1 - \frac{3A_2 \ell}{q}\frac{\partial U}{\partial x}\right)\left(1 - \frac{4A_1 \ell}{q}\frac{\partial U}{\partial x}\right)} + \right.$$

$$\left. + 3q^2 - 18A_1 A_2 \ell^2 \frac{1}{\left(1 - \frac{3A_2 \ell}{q}\frac{\partial U}{\partial x}\right)\left(1 - \frac{4A_1 \ell}{q}\frac{\partial U}{\partial x}\right)} \left|\frac{\partial \mathbb{V}}{\partial z}\right|^2 + 36A_1 A_2 \ell^2 \beta g \times \right.$$

$$\left. \times \frac{1}{\left(1 - \frac{3A_2 \ell}{q}\frac{\partial U}{\partial x}\right)\left(1 - \frac{4A_1 \ell}{q}\frac{\partial U}{\partial x}\right)} \frac{\partial \Theta}{\partial z} \right\} \beta g \frac{\partial \Theta}{\partial z} \tag{13d}$$

$$N = \left(1 - \frac{3A_2 \ell}{q}\frac{\partial U}{\partial x}\right)\left(q^2 + 12A_1 A_2 \ell^2 \beta g \frac{1}{\left(1 - \frac{3A_2 \ell}{q}\frac{\partial U}{\partial x}\right)\left(1 - \frac{4A_1 \ell}{q}\frac{\partial U}{\partial x}\right)} \frac{\partial \Theta}{\partial z}\right) \tag{13e}$$

$$R = \frac{3A_1 \ell}{q}\left\{\left(\overline{u^2} - cq^2\right)\frac{\partial W}{\partial x} + \frac{3A_2 \ell}{q}\beta g\left[\overline{u^2}\frac{\partial \Theta}{\partial x} + \overline{u\theta}\frac{\partial U}{\partial x}\right]\right\} \tag{13f}$$

$$S = \frac{3A_1 \ell}{q}\left\{\overline{uw}\frac{\partial V}{\partial x} + \overline{uv}\frac{\partial W}{\partial x} - \overline{vw}\frac{\partial U}{\partial x} + \frac{3A_2 \ell}{q}\beta g\left[\overline{uv}\frac{\partial \Theta}{\partial x} + \overline{u\theta}\frac{\partial V}{\partial x}\right]\right\} \tag{13g}$$

$$Q = \frac{6A_1^2 \ell^2}{q^2\left(1 - \frac{4A_1 \ell}{q}\frac{\partial U}{\partial x}\right)\left(1 - \frac{3A_2 \ell}{q}\frac{\partial U}{\partial x}\right)}\left(1 - \frac{9A_2^2 \ell^2 \beta g \frac{\partial \Theta}{\partial z}}{1 - \frac{3A_2 \ell}{q}\frac{\partial U}{\partial x}}\right) \tag{13h}$$

$$P = 1 + \frac{12A_1 A_2 \ell^2 \beta g \frac{\partial \Theta}{\partial z}}{q^2\left(1 - \frac{4A_1 \ell}{q}\frac{\partial U}{\partial x}\right)\left(1 - \frac{3A_2 \ell}{q}\frac{\partial U}{\partial x}\right)} \tag{13i}$$

$$\left|\frac{\partial \mathbb{V}}{\partial z}\right|^2 = \left(\frac{\partial U}{\partial z}\right)^2 + \left(\frac{\partial V}{\partial z}\right)^2 \tag{13j}$$

2.2 *The turbulent length scale*

To get the equations (5) to (11) various closures have been used which give us several turbulent length scales λ_1, λ_2, ℓ_1, ℓ_2, Λ_1 and Λ_2. These turbulent length scales are supposed to be proportional to each other. We set $\lambda_1 = \lambda_2 = a_1\ell$, $\ell_1 = A_1\ell$, $\ell_2 = A_2\ell$, $\Lambda_1 = B_1\ell$ and $\Lambda_2 = B_2\ell$, where a_1, A_1, A_2, B_1 and B_2 are constants. For example the dissipation rate ε is parameterized in terms of turbulent energy and some appropriate length scale ℓ

$$\varepsilon = \frac{q^3}{B_1\ell} \tag{14}$$

where $q^2 = \overline{u^2} + \overline{v^2} + \overline{u^2}$.

The principal difficulty with this closure is to determine the ℓ distribution in order to get an accurate dissipation rate. Mellor and Yamada (1974) used Blackadar's (1962) interpolation formula, $1/\ell = \frac{1}{kz} + \frac{1}{\ell_0}$ with $\ell_0 = \alpha \int_0^\infty zq\,dz / \int_0^\infty q\,dz$. This formula interpolates between two limits $\ell = kz$ as $z \to 0$ and $\ell = \ell_0$ as $z \to \infty$. In a convective boundary layer, however, Deardorff's numerical simulation (Deardorff, 1974) with a three dimensional model wherein a portion of the turbulence is explicitly calculated and only the subgrid-scale turbulence needs to be modeled, shows that the ℓ distribution has a maximum in the middle of the convective boundary layer. Furthermore as Yamada's and Mellor's simulation (Yamada and Mellor, 1975), of the Wangara experiment DAY33-DAY35, gave a too shallow depth of the convective boundary layer, we will try another length scale formulation. By using data from measurements in the atmosphere of q^2 and ε one can get an idea of the distribution of ℓ. Let us first look at the distribution of ℓ in the surface layer for different stabilities.

2.2.1 Neutral condition. Surface layer

In neutral conditions data suggest $q^2 = B_1^{2/3} u_*^2$ and $\varepsilon = u_*^3/kz$, thus giving us the turbulent length scale

$$\ell = \frac{q^3}{B_1\varepsilon} = kz \tag{15}$$

2.2.2 Unstable condition. Surface layer

Monin and Yaglom (Monin and Yaglom, 1977) show by theoretical considerations that in near neutral stratification $\varepsilon \approx u_*^3/kz$ and in the case of intense insta-

bility $\varepsilon \approx \sigma \cdot g \cdot \beta \cdot |\overline{w\theta_0}|$, i.e. it becomes independent of the height. σ is a constant. The Kansas measurements (Wyngaard and Coté, 1971) show that under unstable conditions the dissipation data are fairly well represented by

$$\varepsilon = \frac{u_*^3}{kz}\left(1 + 0.5\left|\frac{z}{L}\right|^{2/3}\right)^{3/2} \tag{16}$$

which gives $\varepsilon = u_*^3/kz$ in near neutral stratification and $\varepsilon = 0.35\ g \cdot \beta \cdot \overline{w\theta_0}$ in very unstable stratification. The expression for ε in very unstable stratification can be recast as $\varepsilon\ z_i/w_*^3 = 0.35$ where $w_* = (g\ \overline{w\theta_0}\ \beta \cdot z_i)^{1/3}$.

Analysis of σ_u and σ_v based on several independent field experiments (Panofsky et al., 1977) shows that the standard deviations could be expressed by the following equations

$$\frac{\sigma_u}{u_*} = \frac{\sigma_v}{u_*} = \left(12 + 0.5\ z_i/-L\right)^{1/3} \tag{17}$$

i.e. σ_u and σ_v are not dependent on the height above surface but are dependent only on the height of the convective boundary layer, z_i.

In very unstable stratification

$$\frac{\sigma_u}{u_*} = \frac{\sigma_v}{u_*} = \left(0.5\ k\right)^{1/3} \cdot \frac{1}{u_*}\left(z_i\ \beta g\ \overline{w\theta_0}\right)^{1/3} \tag{18}$$

that is

$$\frac{\sigma_u^2}{w_*^2} = \frac{\sigma_v^2}{w_*^2} = 0.31 \text{ (if von Karman's constant, } k = 0.35) \tag{19}$$

The vertical standard deviation could be expressed by (Panofsky et al., 1977)

$$\frac{\sigma_w}{u_*} = 1.3\left(1 + 3 \cdot z/-L\right)^{1/3} \tag{20}$$

which in very unstable stratification could be rewritten as

$$\frac{\sigma_w^2}{w_*^2} = 1.75\left(\frac{z}{z_i}\right)^{2/3} \tag{21}$$

A free convection prediction based on the Kansas data (Wyngaard et al., 1971) gives in mixing layer similarity form (Kaimal et al., 1976)

$$\frac{\sigma_w^2}{w_*^2} = 1.8 \left(\frac{z}{z_i}\right)^{2/3} \tag{22}$$

The turbulent length scale in the surface layer during unstable conditions can thus be expressed as

$$\ell = \frac{kz}{B_1} \left[\frac{2 \left(12+0.5 \frac{z_i}{|L|}\right)^{2/3} + 1.7 \left(1+3 \frac{z}{|L|}\right)^{2/3}}{1+0.5 \left|\frac{z}{L}\right|^{2/3}} \right]^{3/2} \tag{23}$$

which gives $\ell = kz$ during neutral conditions if $B_1 = 42.5$.

2.2.3 Stable condition. Surface layer

The data from the Kansas experiment (Wyngaard and Coté, 1971) support the following expression for the dissipation rate in stable conditions

$$\frac{kz\ \varepsilon}{u_*^3} = \left[1 + 2.5 \left(\frac{z}{L}\right)^{3/5}\right]^{3/2} \tag{24}$$

Our own turbulent measurements at the Gränby site, Uppsala (Högström et al., 1978) have been further analysed together with new data from measurements at an island, Nässkär, in the archipelago of Stockholm (not yet published) with respect to the total turbulent energy. In Fig 1 mean values of q^2/u_*^2 for different stability classes are plotted. The full line in that figure represents the equation

$$\frac{q^2}{u_*^2} = \left[\frac{B_1(1+3.7\ z/L)}{1+1.7\ z/L}\right]^{2/3} \tag{25}$$

which is forced to go through the value $\frac{q^2}{u_*^2} = B_1^{2/3}$ at $z/L = 0$ matching it with the expression of q^2/u_*^2 for unstable conditions, see above.

From these two expressions of the dissipation and the turbulent energy we may form the following length scale

$$\ell = kz \frac{1+3.7\ z/L}{\left(1+1.7\ z/L\right)\left(1+2.5\ (\frac{z}{L})^{3/5}\right)^{3/2}} \tag{26}$$

For large z/L, i.e. very strong stable stratification, this expression for ℓ could be recast as

$$\ell = 0.2\ L^{9/10}\ z^{1/10} \tag{27}$$

which means that the turbulent length scale has a tendency to become more or less independent of z (Tennekes, 1982).

The Kansas results (Wyngaard and Coté, 1971) show that the flux divergence term in the budget of turbulent kinetic energy is neglible in the surface layer. This implies that for quasi-stationary and horizontally homogeneous conditions

$$\varepsilon = -\overline{uw}\ \frac{\partial U}{\partial z} + \beta g\ \overline{w\theta} \tag{28}$$

but

$$-\overline{uw} = u_*^2 \tag{29}$$

$$\frac{\partial U}{\partial z} = \frac{u_*}{kz}\ \phi_m \tag{30}$$

$$\beta g\ \overline{w\theta} = -\frac{u_*^3}{Lk} \tag{31}$$

which implies

$$\frac{\varepsilon\ kz}{u_*^3} = \phi_m - \frac{z}{L} = 1+3.7\ z/L \tag{32}$$

If we use this expression for ε when determining the turbulent length scale we get

$$\ell = \frac{kz}{1+1.7\ z/L} \tag{33a}$$

which for large z/L becomes

$$\ell = 0.2\ L \tag{33b}$$

i.e. no dependence on z.

The Kansas results also show that the flux divergence term in the budget of the temperature variance is neglible in the surface layer during stable conditions. Eq (6) then gives us

$$\overline{\theta^2} = \frac{B_2 \ell_2}{q} (-\overline{w\theta}) \frac{\partial \Theta}{\partial z} \tag{34}$$

for quasi-stationary and horizontally homogeneous conditions. ℓ_2 is a length scale for dissipation of $\overline{\theta^2}$. But in the surface layer we have

$$\frac{\partial \Theta}{\partial z} = \frac{\theta_*}{kz} \phi_h \tag{35}$$

$$q^2 = B_1^{2/3}\ u_*^2 \left(\frac{1+3.7\ z/L}{1+1.7\ z/L}\right)^{2/3} \quad \text{(see above, Eq (25))}$$

Let us now suppose

$$\ell_2 = kz/\phi_\Theta \tag{36}$$

where ϕ_Θ is a universal function of z/L. This implies

$$\overline{\theta^2} = B_2 \theta_*^2\ B_1^{-1/3} \left(\frac{1+3\ z/L}{1.1.7\ z/L}\right)^{-1/3} \phi_h\, \phi_\Theta^{-1} \tag{37}$$

The measurements in Kansas (Wyngaard et al., 1971) indicate that $\overline{\theta^2}/\theta_*^2$ is a constant in the stable surface layer ≈ 3.2. Other measurements including laboratory experiments indicate $\overline{\theta^2}/\theta_*^2 \approx 3.1$ (Yamada, 1979). If B_1 and B_2 are constants and B_2 is defined as $u_*^2\ \overline{\theta^2}/\overline{w\theta^2}\ B_1^{1/3}\ P_{rt}^{-1}$, where P_{rt} is Prandtl's number, this gives,

$$\phi_\Theta = \frac{1}{P_{rt}} \left(\frac{1+1.7\ z/L}{1+3.7\ z/L}\right)^{1/3} \phi_h \approx 1+4.9\ z/L \tag{38}$$

and $B_2 = 15.1$.

This implies that the turbulent length scale of the temperature variance differs from the length scale of the turbulent energy. To numerically simplify the model we have supposed the length scales to be proportional to each other in the present version of the model hoping this will not affect the result too seriously. The difference between the length scales determined from Eq (26) and Eq (27) respectively, is less than the difference between the length scale for the turbulent energy and the length scale for the temperature variance. We will therefore use a length scale being a mean of the more simple form Eq (33) and the length scale for the temperature variance, Eq (36), giving us

$$\ell = kz/\left(1+3.3\ z/L\right) \tag{39}$$

2.2.4 Unstable condition. Transition layer

For the convective boundary layer we will use data from the Ashchurch (Caughey and Palmer, 1979) and the Minnesota (Izumi and Caughey, 1976) experiments and Willis' and Deardorff's experiment (Willis and Deardorff, 1974) to get an expression for the turbulent length scale. The dimensionless vertical velocity variance is about 0.1 near the surface and has a broad maximum of about 0.4 in the middle of the layer and decreases to about 0.1-0.2 at $z = z_i$ (Caughey, 1982). We want to express the measured data analytically.

$$\frac{\sigma_w^2}{w_*^2} = 1.8\left(\frac{z}{z_i}\right)^{2/3} - 1.65\left(\frac{z}{z_i}\right)^{4/3} \tag{40a}$$

is the equation for the full line curve in Fig 2, which fits the atmospheric data and the tank experiment data fairly well. Near the surface this line approaches the free convection prediction

$$\frac{\sigma_w^2}{w_*^2} = 1.8\left(\frac{z}{z_i}\right)^{2/3} \tag{40b}$$

The longitudinal and lateral components of the dimensionless velocity variances in the convective boundary layer seem to fit the unstable limit prediction from the surface layer data quite well, see Eq (19)

$$\frac{\sigma^2_{u,v}}{w_*^2} = 0.31 \tag{41}$$

see Fig 3.

This means that the turbulent energy in the convective boundary layer can be approximated as

$$q^2/w_*^2 = \left(2 \cdot 0.31 + 1.8 \left(\frac{z}{z_i}\right)^{2/3} - 1.65 \left(\frac{z}{z_i}\right)^{4/3}\right) \tag{42}$$

The normalized dissipation rate shows some indication of a slight decrease with height according to the Ashchurch and the Minnesota experiments (Caughey, 1982). The full line curve in Fig 4 is

$$\frac{\varepsilon z_i}{w_*^3} = 0.6 \left(\frac{z}{z_i}\right)^{-1/3} - 0.3 \tag{43}$$

which fits the data fairly well. From Eqs (42) and (43) we may now obtain a mixing length for unstable stratification

$$\ell = \frac{\left(0.62 + 1.8 \left(\frac{z}{z_i}\right)^{2/3} - 1.65 \left(\frac{z}{z_i}\right)^{4/3}\right)^{3/2} z_i}{B_1 \left(0.6 \left(\frac{z}{z_i}\right)^{-1/3} - 0.3\right)} \tag{44}$$

2.2.5 Stable condition. Transition layer

As measurements in surface layer during stable conditions support the theory that the turbulent length scales have a tendency to become more or less independent of z when z/L is increasing, see section 2.2.3, we extend Eq (39) to be applicable to the atmosphere above surface layer if the surface layer is stable. If the surface layer is unstable instead Deardorff (1974) shows with his three dimensional model that the turbuelnt length scale is constant between z_i and 1.2 z_i. Above $1.2z_i$ ℓ is increasing rapidly which is indicative of internal gravity waves containing kinetic energy but undergoing less and less diffusion or turbulent breakdown with increasing height (Deardorff, 1974). As it is dif-

ficult to get an expression for this increase of the turbulent length scale above $1.2z_i$ we suppose in the present version of the model a constant value of ℓ, $\ell = \ell(z_i)$ above $z = z_i$.

2.2.6 Near neutral condition

We define near neutral conditions as $|H/L| < 10$ where H is equal to $0.2\ u_*/f$ in stable conditions and $H = z_i$ in unstable conditions. If $|H/L| < 10$ and we have unstable conditions, we use the same expression for ℓ we got from the mixing layer scaling, Eq (44), but with $0.2\ u_*/f$ instead of z_i. If we have a neutral or stable surface layer and $|H/L| < 10$ the characteristic length is taken as Delage (1974) length

$$1/\ell = \frac{1}{kz} + \frac{\beta}{kL} + \frac{1}{\lambda} \tag{45}$$

where $\lambda = 0.1\ H$.

To get the constant β we have matched Eq (45) for $H/L = 10$ against Eq (39), which gives $\beta = 3.0$.

2.3 *The model coefficients*

As mentioned above all the length scales are assumed to be proportional to each other. The length scales are, see Eq (5) - Eq (9):

$$(\lambda_1,\ \lambda_2,\ \ell_1,\ \ell_2,\ \Lambda_1,\ \Lambda_2) = (a_1\ell,\ a_2\ell,\ A_1\ell,\ A_2\ell,\ B_1\ell,\ B_2\ell)$$

where the constant a_1, a_2, A_1, A_2, B_1 and B_2 have to be determined. Additionally we have to determine the constant c in Eqs (7) - (9).

The constants B_1 and B_2 are already determined, see above, to 42.5 and 15.1 respectively.

As shows by Mellor (1973) the constants A_1, A_2, B_1, B_2 and c are dependent on each other. In neutral horizontally homogeneous conditions Eqs (7) and (8b) may be written for the surface layer, after some algebra, as

$$\overline{u^2} = (1-2\gamma)\ q^2 \tag{46}$$

$$\overline{v^2} = \gamma\ q^2 \tag{47}$$

$$\overline{w^2} = \gamma\ q^2 \tag{48}$$

$$A_1 = B_1(1/3-\gamma)/2 \tag{49}$$

$$C = \gamma - (3A_1B_1^{1/3})^{-1} \tag{50}$$

$$A_2 = A_1(\gamma-c)\ (\gamma P_r)^{-1} \tag{51}$$

As seen from Eqs (47) and (48) the closure we have used support that $\overline{v^2} = \overline{w^2}$ but measurements in the atmosphere instead support $\overline{u^2} \approx \overline{v^2}$. We will therefore use Eq (46) to determine the constant γ. Measurements in the surface layer give according to Eq (17) and (20) $\overline{u^2}/\overline{q^2} = 0.43$ in neutral conditions. From Eq-s (46)-(51) we then get

$$\gamma = 0.2848$$

$$A_1 = 1.031$$

$$A_2 = 0.4532$$

$$C = 0.1922$$

To determine the constant a_2 used in the equation for the temperature variance we will look at the closure used for $\overline{w\theta^2}$. In equation (6) we have supposed that

$$\overline{w\theta^2} = -q\,\lambda_2 \frac{\partial\overline{\theta^2}}{\partial z} \tag{52}$$

Instead let us now look at the equation

$$\overline{w\theta^2} = -\sqrt{\overline{w^2}}\,\lambda_w \frac{\partial\overline{\theta^2}}{\partial z} \tag{53}$$

where

$$\lambda_w = a_w \ell \tag{54}$$

The free convection predictions for $\overline{w\theta^2}$, $\overline{\theta^2}$ and $\overline{w^2}$ (Wyngaard et al., 1971) expressed in mixing layer similarity parameters are

$$\overline{w\theta^2} = 1.1\,w_*\,\theta_*^2\,(\frac{z}{z_i})^{-1/3} \tag{55}$$

$$\overline{\theta^2} = 1.8\,\theta_*^2\,(\frac{z}{z_i})^{-2/3} \tag{56}$$

$$\overline{w^2} = 1.8\,w_*^2\,(\frac{z}{z_i})^{2/3} \tag{57}$$

According to Fig 14 in Kaimal et al, 1976 the local free convection predictions seem to fit the measurements fairly well in the lower part of the convective boundary layer which allow us to use these expressions in determining the constant a_w in Eq (54).

From Eq (56) we get

$$\frac{\partial\overline{\theta^2}}{\partial z} = -\frac{2}{3}\,1.8\,\theta_*^2\,z_i^{2/3}\,z^{-5/3} \tag{58}$$

Eqs (55), (57) and (58) in Eq (52) and using $\ell = kz$ give

$$a_w = \frac{1.1 \cdot 3}{2 \cdot 1.8 \cdot 0.35\,\sqrt{1.8}} = 1.95 \tag{59}$$

But since we have used Eq (52) as the closure for $\overline{w\theta^2}$ in Eq (6) we have to determine the ratio $\sqrt{\overline{w^2}}/q$ in very unstable conditions. In a convective surface boundary layer Eq (7c) can be approximated as

$$\overline{w^2} = \frac{q^2}{3} + 4\,\frac{\ell_1}{q}\,\beta g\,\overline{w\theta} \tag{60}$$

At the same time q^3 can be approximated from Eq (5) in surface layer and during very unstable conditions as

$$q^3 = B_1\,\ell\,\beta g\,\overline{w\theta} \tag{61}$$

From Eqs (60) and (61) we now get

$$\frac{\overline{w^2}}{q^2} \approx \frac{1}{3} + \frac{4A_1}{B_1} \tag{62}$$

which gives us

$$a_2 = a_w\sqrt{\frac{\overline{w^2}}{q^2}} = 1.28 \tag{63}$$

To get a value of a_1 we simply assume $a_1 = a_2$.

In the calculations above we have used $\ell = kz$ as the length scale for the surface layer but according to Eq (23) $\ell > kz$ in an unstable surface layer which means that $a_2 < 1.28$. Lewellen and Teske (1975) have chosen the diffusion length

scale as 0.3•1.68 kz close to the wall which gives $a_2 = 0.5$. Their value is based on computer studies of jets and wakes. Yamada & Mellor (1973) have chosen the diffusion coefficient equal to 0.23. Their value is based on calculations on channel flows and a constant pressure boundary layer (Mellor and Herring, 1973). As the constant is difficult to determine we have carried out several simulations of the Wangara data for the convective boundary layer. The simulations of the second order moments show best agreement with Deardorff's 3-D model results and with atmospheric data if we use a constant around 1.

2.4 *Boundary conditions*

In the surface layer the wind components can be expressed as

$$U = \frac{u_*}{k}\left(\ln\frac{z}{z_0} - \Psi_m\right)\cos\alpha \tag{64a}$$

$$V = \frac{u_*}{k}\left(\ln\frac{z}{z_0} - \Psi_m\right)\sin\alpha \tag{64b}$$

where $\ln z/z_0 - \Psi_m = \int_{z_0}^{z} \phi_m\left(\frac{z}{L}\right)/z\, dz$, ϕ_m is the nondimensional wind gradient.

At the two lowest grid points we can form the following relations for U and V from these equations

$$\frac{U_1}{U_2} = \frac{\ln z_1/z_0 - \Psi_{m_1}}{\ln z_2/z_0 - \Psi_{m_2}} \tag{65a}$$

$$\frac{V_1}{V_2} = \frac{\ln z_1/z_0 - \Psi_{m_1}}{\ln z_2/z_0 - \Psi_{m_2}} \tag{65b}$$

These relations provide a finite difference boundary condition for velocity at the lower boundary.

We get the boundary condition for temperature from the measured value of the temperature at 'screen height', $z_m = 1.2$ m. In the surface layer the temperature can be expressed as

$$\Theta = \theta_0 + \frac{\Theta_*}{k}\left(\ln z/z_{oT} - \Psi_\Theta\right) \tag{66}$$

where $\ln z/z_{oT} - \Psi_\Theta \int_{z_{oT}}^{z} \phi_h \, dz$, ϕ_h is the nondimensional temperature gradient.

For the first grid point and for the 'screen height', z_m we then have

$$\Theta_1 = \Theta_0 + \frac{\Theta_*}{k}\left(\ln z_1/z_{oT} - \Psi_{\Theta_1}\right) \tag{67a}$$

$$\Theta_m = \Theta_0 + \frac{\Theta_*}{k}\left(\ln z_m/z_{oT} - \Psi_{\Theta_m}\right) \tag{67b}$$

From these two equations we get

$$\Theta_1 = \Theta_m - \frac{\Theta_*}{k}\left(\ln z_m/z_{oT} - \Psi_{\Theta_m}\right) + \frac{\Theta_*}{k}\left(\ln z_1/z_{oT} - \Psi_{\Theta_1}\right) \tag{68}$$

which gives us the temperature at the first grid point from the measured one at the 'screen height'.

To get Ψ_m and Ψ_Θ from the ϕ_m and ϕ_h expressions we have applied Paulsson (1970). The ϕ_m and ϕ_h expressions used are from the Kansas measurements (Wyngaard et al., 1971). The surface boundary conditions for q^2 are according to Panofsky et al., (1977) in unstable conditions

$$q_1^2 = u_*^2\left(2(12+0.5\,\frac{z_i}{-L})^{2/3} + 1.7(1+3\,\frac{z_1}{-L})^{2/3}\right) \tag{69a}$$

and from our own measurements in stable conditions, (Eq (25)),

$$q_1^2 = u_*^2\left(B_1\,\frac{1+3.7\ z_1/L}{1+1.7\ z_1/L}\right)^{2/3} \tag{69b}$$

where $B_1 = 42.5$.

According to Wyngaard et al., (1971) $\overline{\theta^2}/T_*^2$ seems to be a constant in stable air. It seems to fit the local free convection prediction very well for $z/L < -0.15$.

For $z/L = -0.15$ the free convection prediction $\overline{\theta^2}/T_*^2 = 0.90\ (-z/L)^{-2/3}$ gives the same value for $\overline{\theta^2}/T_*^2$ as in stable conditions. The surface boundary conditions for $\overline{\theta^2}$ is therefore taken as

$$\overline{\theta_1^2} = T_*^2 \cdot 0.90\left(-z/L\right)^{2/3} \qquad \text{for } z/L < -0.15 \tag{70a}$$

$$\overline{\theta_1^2} = T_*^2 \cdot 3.2 \qquad \text{for } z/L > -0.15 \tag{70b}$$

At the upper boundary we have set

$$\frac{\partial q^2}{\partial z} = \frac{\partial \overline{\theta^2}}{\partial z} = \frac{\partial U}{\partial z} = \frac{\partial V}{\partial z} = 0 \qquad (71)$$

We assume for temperature that the derivative at the top is equal to the derivative at the grid point below the top.

For the upstream and downstream boundary conditions we have simply supposed that the derivatives in the x-direction are equal to zero.

2.5 *Initial conditions*

As initial profiles for the U- and V-components we use the geostrophic wind for $z > 100$ m. Below 100 m we assume neutral conditions to exist and use a logarithmic profile for U and V. For temperature we use measured values for the initialisation. The model generates q^2 and $\overline{\theta^2}$ profiles after about 1 hour integration time, by keeping wind and temperature profiles constant.

2.6 *The geostrophic wind*

The surface geostrophic wind (U_{g_0}, V_{g_0}) and the thermal winds from the surface to the height Z1 and from the height Z1 to the height Z2 are given for certain time intervals. Following Yamada and Mellor (1975) parabolic profiles are fitted to these values so that the eastward geostrophic wind component for example is given by the expression

$$U_g(z) = \left(\frac{(\Delta U_g)_2}{Z2(Z2-Z1)} - \frac{(\Delta U_g)_1}{Z1 \cdot Z2}\right) z^2 + \left(\frac{Z1+Z2}{Z1 \cdot Z2}(\Delta U_g)_1 - \frac{Z1}{Z2(Z2-Z1)}(\Delta U_g)_2\right) z + U_{g_0} \qquad (72)$$

where $(\Delta U_g)_1$ and $(\Delta U_g)_2$ are the thermal wind differences from surface up to level Z1 and from level Z1 up to level Z2, respectively. The values for U_{g_0}, V_{g_0}, $(\Delta U_g)_1$, $(\Delta U_g)_2$, $(\Delta V_g)_1$ and $(\Delta V_g)_2$ at times between observations are linearly interpolated.

2.7 *The grid system and the finite-difference scheme*

The equations (1)-(6) are transformed into a new coordinate system (x,y,ζ) where ζ is defined through the relation

$$\zeta = a_1 z + a_2 \ln (z/a_3) \qquad (73)$$

where a_1, a_2 and a_3 are constants

$$a_3 = \exp\left(\left[(N\cdot\Delta\zeta - ZT)\cdot\ln(Z1) - (\Delta\zeta - Z1)\cdot\ln(ZT)\right] / N\cdot\Delta\zeta - ZT - \Delta\zeta + Z1\right)$$

$$a_2 = (\Delta\zeta - Z1)/\ln(Z1/a_3)$$

$$a_1 = 1$$

$\Delta\zeta = 50\cdot(60/N)$

N = number of grid points in z-direction

ZT = the height of the model

Z1 = the height to the first grid point

The grid points are equally spaced in ζ.

In the tests presented in this report we have used 30 grid points in the z-direction and 2000 m as the height of the model. The lowest grid point is set to 0.5 m which gives

$a_3 = 0.200$

$a_2 = 108.5$

Table 1. The physical heights of the grid points used.

Grid nr	Height z (m)	Grid nr	Height z (m)
1	0.50	16	712.12
2	1.25	17	799.54
3	3.08	18	888.14
4	7.43	19	977.70
5	17.09	20	1068.10
6	36.04	21	1159.21
7	67.66	22	1250.95
8	112.48	23	1343.22
9	168.56	24	1435.97
10	233.28	25	1529.14
11	304.39	26	1622.70
12	380.24	27	1716.59
13	459.65	28	1810.79
14	541.80	29	1905.27
15	626.09	30	2000.00

Wind and temperature are calculated on these grid points, but turbulent energy and temperature variances are calculated on grid points $\frac{1}{2}\Delta\zeta$ below the grid points for wind and temperature.

The grid distances in the x-direction are different for different tests. The grid distances used for the several tests are given in section 3.

Before applying a finite-difference scheme on equations (1)-(6) a complex equation is formed from Eq (1) and Eq (2) giving

$$\frac{\partial \hat{V}}{\partial t} + U\frac{\partial \hat{V}}{\partial x} + W\frac{\partial \hat{V}}{\partial z} = -\,if\,(\hat{V}-\hat{V}_g) + \frac{\partial}{\partial z}\left(K_M\frac{\partial \hat{V}}{\partial z}\right) + \frac{\partial}{\partial z}\left(\tau_a + i\tau_b\right) +$$

$$+ \frac{\partial}{\partial x}\left(-\overline{u^2} - i\,\overline{uv}\right) \qquad (74)$$

where we also have used Eqs (10a) and (10b) and where $\hat{V} \equiv U + iV$ and $\hat{V}_g \equiv U_g + iV_g$. All the equations can be reduced to a general expression, namely

$$\frac{\partial \phi}{\partial t} = \frac{\partial}{\partial z}\left(K\frac{\partial}{\partial z}\right) - R\frac{\partial \phi}{\partial z} - P\cdot\phi + F \qquad (75)$$

Table 2 identifies ϕ, K, R, P and F.

Table 2.

ϕ	K	R	P	F
$\hat{V}$	K_M	w	if	$if\hat{V}_g + \frac{\partial}{\partial z}(\tau_a + i\tau_b) + \frac{\partial}{\partial x}(-\overline{u^2} - i\,\overline{uw}) - U\frac{\partial \phi}{\partial x}$
Θ_v	K_H	w	o	$\frac{fT_v}{g}\left(V\frac{\partial U_g}{\partial z} - U\frac{\partial V_g}{\partial z}\right) + \sigma_r - \frac{\partial \tau_c}{\partial z} + \frac{\partial}{\partial x}(-\overline{u\theta}) - U\frac{\partial \Theta}{\partial x}$
$\frac{q^2}{2}$	$\frac{5}{3}q\lambda_1$	w	$\frac{q}{\Lambda_1}$	$-\frac{1}{2}U\frac{\partial q^2}{\partial x} - \overline{uw}\frac{\partial U}{\partial z} - \overline{vw}\frac{\partial V}{\partial z} - \overline{u^2}\frac{\partial U}{\partial x} - \overline{uv}\frac{\partial V}{\partial x} - \overline{uw}\frac{\partial W}{\partial x} - \overline{w^2}\frac{\partial W}{\partial z} + \beta g\,\overline{w\theta} - \frac{\partial}{\partial x}K\frac{\partial}{\partial x}\frac{q^2}{2}$
$\frac{\overline{\theta^2}}{2}$	$q\lambda_3$	w	$\frac{q}{\Lambda_2}$	$-\overline{w\theta}\frac{\partial \Theta}{\partial z} - U\frac{\partial}{\partial x}\frac{\overline{\theta^2}}{2} - \overline{u\theta}\frac{\partial \Theta}{\partial x} - \frac{\partial}{\partial x}K\frac{\partial}{\partial x}\frac{\overline{\theta^2}}{2}$

We have employed a difference scheme by Laasonen (Richtmyer et al., 1967). The equation system has been solved with the aid of a recursion formula (Richtmyer et al., 1967).

3 TESTS

To test the model we will first use a one-dimensional version of it and test it against the Wangara data (DAY33-DAY35), (Clarke et al., 1971). We will compare the mean variables (U, V and Θ) with the measured values. The turbulence quantities are compared with normalized data from other sites, water tank experiments and three-dimensional models in convective conditions.

As indata to the model we have used only the temperature variation at 'screen height' and the geostrophic wind at ground, 1000 m and 2000 m and an initial profile for temperature. The integration starts at 0900 DAY33 and ends at 0800 DAY35.

3.1 *Mean temperature, heat flux and temperature fluctuations*

In Figs 5a-b the computed and observed profiles of the mean potential temperature are compared at different times on DAY33. The observed temperature seems to have been simulated very well by the model during daytime DAY33. In the present model no radiation scheme is included. But during daytime, when we have a convective layer, the flux divergence is negligible compared with the divergence of turbulent flux of sensible heat. As we give the temperature profile at 0900 DAY33 as a start profile, the divergence of the radiative flux will not affect the result. In Figs 6a-b the computed and observed profiles of the mean potential temperature are compared at different times on DAY34. Here we see that the result is poorer. The computed temperature at 0900 DAY34 is several degrees higher than observed in the region 50-700 m. This is probably caused by the influence of the radiative cooling during night-time. At screen height the real temperature is given, which means that the temperature will be correct near the surface.

The time and space variations of the computed and observed mean potential temperature are shown in Fig 7. We also see here that during night-time we get a too shallow surface inversion layer, probably due to the fact that we have excluded the flux divergence of longwave radiation in the model.

In a convective layer the heat flux $\overline{w\theta}$ is a linear function of height (see Deardorff, 1974 and André et al., 1978). The kinematic heat flux has been made dimensionless by its surface value and is plotted against the dimensionless height z/z_i in Fig 8 and Fig 9 for DAY33 and DAY34, respectively. An extrapolation of the linear flux sections to height z_i in the Figs 8-9 reveals that the

ratio of maximum negative heat flux to the surface heat flux equals ≈ 0.15. Willis and Deardorff (1974) gives values of 0.23 for experiment S1 and 0.11 for experiment S2. The numerical model of Wyngaard and Cotē (1974) gives the value 0.1, while Deardorff's 3-D model (Deardorff, 1974) gives this ratio to about 0.18 as a mean value.

The temperature variance can be made dimensionless by $T_*^2 = Q_0^2/w_*^2$ (Willis and Deardorff, 1974). The dimensionless profiles of potential temperature variance are shown in Fig 10 and Fig 11 for DAY33 and DAY34 respectively and we can notice that the normalized temperature variance profiles are almost stationary during convective conditions. The normalized temperature variance decreases rapidly with height and the present model gives a minimum of ~ 2.0 at around $z/z_i = 0.75$. The Minnesota experiment (Izumi and Caughey, 1976) and the Ashchurch experiment (Caughey and Palmer, 1979) as well as Deardorff's 3-D model (1974) have a broad minimum of 2-3 at around $z/z_i = 0.7$. Near the top of the convective boundary layer the temperature variance do not scale with T_*^2. This effect, already noted by Deardorff (1974) and André et al., (1976), is due to an increasing temperature jump at the inversion level which induces a larger vertical inhomogeneity of temperature.

3.2 *Mean wind and velocity fluctuations*

In Figs 12-15 computed wind profiles are compared with observed ones. We notice that during daytime, when we have a convective layer, the wind profiles are nearly constant with height which is a result of strong turbulent mixing. During the night we have a low level jet (nocturnal jet), with maximum wind-speed at around 200-300 m height. The momentum fluxes are negligible in the upper parts of the boundary layer. This implies that any discrepancy between observed values and the strictly inertial motion computed from the wind equation (57) with $\overline{uw} = \overline{vw} = 0$ must be due to the fact that synoptic scale advection is not included in the model. To test if it is this kind of error that gives the large discrepancy between observed and computed wind-speed, especially during DAY34 above 500 m, we have inserted an advection term in the wind equation by making the following assumptions. Above 500 m we assume that the advection terms $U\frac{\partial U}{\partial x}$, $V\frac{\partial U}{\partial y}$, $U\frac{\partial V}{\partial x}$ and $V\frac{\partial V}{\partial y}$ can be approximated with $U\frac{\partial U_g}{\partial x}$, $V\frac{\partial U_g}{\partial y}$, $U\frac{\partial V_g}{\partial x}$ and $V\frac{\partial V_g}{\partial y}$ respectively. The whole pressure field (see Clarke et al., 1971) is moving SE between DAY33 and DAY34 with a speed of around $U_x = 4.5$ m/s in x-direction and $U_y = -4.5$ m/s in y-direction. This means that we can approximate δx and δy with

$U_x \delta t$ and $U_y \delta t$ respectively. The advection terms can then be approximated as

$$U \frac{\partial U}{\partial x} \approx \frac{U}{U_x} \frac{\partial U_g}{\partial t} \tag{76a}$$

$$V \frac{\partial U}{\partial y} \approx \frac{V}{U_y} \frac{\partial U_g}{\partial t} \tag{76b}$$

$$U \frac{\partial V}{\partial x} \approx \frac{U}{U_x} \frac{\partial V_g}{\partial t} \tag{76c}$$

$$V \frac{\partial V}{\partial y} \approx \frac{V}{U_y} \frac{\partial V_g}{\partial t} \tag{76d}$$

Below 500 m we cannot approximate the advection terms in this manner. Instead we assume that the $\frac{\partial}{\partial x}$ - and $\frac{\partial}{\partial y}$ -terms decrease linearly downwards from z = 500 m to zero at surface. Fig 16 and Fig 17 present wind profiles for the nights of DAY34 and DAY35, respectively, obtained with the model and with these assumptions included. We can compare these profiles with the measured ones and those computed without the advection terms and see that the new profiles give a much more realistic result, (Fig 16 should be compared with Figs 13 a-b and Fig 17 with Figs 15 a-b).

In Fig 18 the time and space variation of the eastward mean wind component U is drawn and in Fig 19 the northward component V. The computed wind components are determined with the synoptic advection terms included in the equations and we can see that the model simulates the wind field quite well.

In determining a proper turbulent length scale we have used atmospheric measurements of the dissipation rate and of the turbulent energy. If all constants and all other closures are correct the simulations of the second order moments should agree with the measured ones used in the definition of the length scale.

The velocity fluctuations $\overline{u^2}$, $\overline{v^2}$ and $\overline{w^2}$ could be made dimensionless by $w_* = (\beta g \, Q_0 z_i)^{1/3}$ in a convective boundary layer (Deardorff, 1970). The dimensionless profiles of the eddy kinetic energy components are presented in Fig 20 and Fig 21 for the vertical standard deviation component and in Fig 22 for the horizontal velocity standard deviations. Here we can notice that $\overline{w^2}$ do scale with w_*^2 but the agreement is much better during DAY33 than during DAY34. On DAY33 we get a maximum of ≈ 0.49 at $z \approx 0.3 \, z_i$. We get the maximum at the same height as in Deardorff's model (Deardorff, 1974) and André's model (André et al., 1978),

but the maximum value is about 0.49 in the present model compared with 0.44 according to Deardorff's model.

The dashed line in Fig 20 is the local free convection curve according to extrapolation of very unstable surface layer observations (Wyngaard et al., 1971). Atmospheric measurements and Deardorff's 3-D model show that the vertical energy component agree with the local free convection prediction in the lowest part of the convective boundary layer. It seems that the present model overestimates $\overline{w^2}$ near the lower boundary. The energy of the horizontal components, here taken as the mean of $\overline{u^2}$ and $\overline{v^2}$, also seems to scale fairly well with w_*^2, see Fig 22. Deardorff's 3-D model (1974) and André's model (1976) carrying differential equation for the third moments as well and measurements in the atmosphere (Izumi and Caughey, 1976 and Caughey and Palmer, 1979) suggest that the horizontal energy components are nearly constant with height above 0.2 z_i. Deardorff gives a value $\overline{e}_h \sim 0.15\ w_*^2$ André $\overline{e}_h \sim 0.2\ w_*^2$ and measurement $\sim 0.35\ w_*^2$. The present model gives this value to about $0.25\ w_*^2$. Below 0.2 z_i the horizontal energy components decreases with height according to Deardorff's model as well as André's model. In the present model the horizontal energy components are constant with height in this region. The total turbulent energy profiles are similar in shape for the present model and Deardorff's model. That means that the analytical expressions, Eqs (7a)-(7c), give too much energy into the vertical component in the lowest part of the convective boundary layer and underestimate the horizontal components.

3.3 *Height of the mixed layer*

The evolution of z_i, defined as the height where $\overline{w\theta}$ has its minimum, is shown in Fig 23. Both during DAY33 and DAY34 the height z_i is very well simulated when we have a fully developed convective boundary layer but the mixing height grows too slowly the first hour. Probably, as pointed out in the section 3.1, this is due to the missing radiation divergence term in the temperature equation.

3.4 *Sensitivity tests*

When parameterizing the third order moments in our set of equations we get a number of length scales that have to be determined. In the present model we have supposed these length scales to be proportional to each other, which means that we only have to determine one length scale and a certain number of proportionality factors. Some of these constants have been determined from measurements in

the surface layer and other constants are related to these first constants. The most difficult constants to determine are the diffusion coefficients a_1 and a_2. Simulations of the Wangara data have been performed for several different values of a_1 and a_2, but in all tests a_1 is set equal to a_2. In the simulations above $a_1 = a_2 = 1$. Yamada and Mellor have supposed that $a_1 = a_2 = 0.23$. Our simulations give much poorer results for the second order moments in a convective boundary layer with this latter constant. A shown example is the variation of the simulated horizontal energy components with the height, z/z_i. Fig 24 shows this variation using $a_1 = a_2 = 0.23$ in the simulations. This figure should be compared with Fig 3 showing results from atmospheric measurements and Deardorff's 3-D model and with Fig 22 showing the results from the present model where $a_1 = a_2 = 1.0$. There is very little difference between simulations of the second order moments if we choose the diffusion constant between 0.8 and 1.3. At the same time the simulations show that the mean variables seem not to be influenced by the constant. We get about the same mean wind and mean temperature field if we use $a_2 = 0.23$ or $a_2 = 1.3$.

3.5 *Test of the two-dimensional version of the model*

To test the two-dimensional version of the model we have used data from measurements in the island of Gotland, Sweden (Faxén, 1980). The wind measurements which consisted of pilot baloon trackings, were performed at five places in Gotland: Näsudden, Eksta, Ygne, Lojsta and När, see Fig 25. As the model is two-dimensional with only one horizontal axis we project the measurement sites on the x-axis. This is performed so that the distance between the west coast of Gotland and the measurement sites and corresponding grid distances agree, see Table 3 and Fig 25. The roughness lengths used are also given in the table.

Grid points 1-4 are supposed to give the conditions over the sea west of Gotland. Among the grid points in Gotland Näsudden corresponds to grid point 5, Eksta to grid point 6, Lojsta to grid point 16 and När to grid point 26.

We will test the model against measurements performed 21-23 November 1978. The measurements started about 8 GMT in the morning but the simulations start at 6 GMT with the purpose that the results will not be too much dependent on the start profiles of wind and temperature needed. The initial temperature profile — — equal in all x-grid points — is taken as the temperature profile gotten from the radiosonde measurements at 12 GMT outside Visby.

Table 3. Grid distances in x-direction and the roughness lengths used.

Gridpoint nr	Distance from gridpoint 1 (km)	z_o (m)	Gridpoint nr	Distance from gridpoint 1 (km)	z_o (m)
1	0.0	0.00024	16	21.7	0.8
2	2.0	0.00024	17	23.1	0.3
3	4.0	0.00024	18	24.5	0.3
4	6.0	0.00024	19	25.9	0.3
5	7.2	0.1	20	27.3	0.3
6	8.5	0.5	21	28.7	0.3
7	9.8	0.5	22	30.1	0.3
8	11.1	0.5	23	31.5	0.2
9	12.4	0.5	24	32.9	0.2
10	13.7	0.8	25	34.4	0.2
11	15.0	0.8	26	35.7	0.1
12	16.3	0.8	27	38	0.00024
13	17.6	0.8	28	40	0.00024
14	18.9	0.8	29	42	0.00024
15	20.2	0.8	30	44	0.00024

The initial profiles for the wind are also equal in all x-grid points and are taken as the geostrophic wind profile. The geostrophic wind is taken from surface maps, 850 mbar and 750 mbar maps. The geostrophic wind-speed and direction used in the simulations are given in table 4.

Table 4. The geostrophic wind-speed and direction at Gotland 21-24 november 1978.

Date	Time (GMT)	Surface (m/s)	Surface (^{o})	850 mbar (m/s)	850 mbar (^{o})	750 mbar (m/s)	750 mbar (^{o})
21/11	0	11.4	270	10.8	285	16.2	280
	12	17.2	250				
22/11	0	20.0	270	17.3	270	19.5	270
	12	16.0	300				
23/11	0	30.3	290	35.1	280	27.4	280
	12	16.0	300				
24/11	0	13.4	270	15.8	280	19.2	290

As the temperature at screen height, which we would like to use as the lower boundary for temperature, was not measured on the different grid points or

either at the measurement sites, we have to use another type of boundary condition for the temperature. We have used synoptic weather stations at Stora Karlsö, west of Gotland, and at Herrvik, at the east coast of Gotland, Fig 25.

The synoptic station at Stora Karlsö is supposed to give the temperature changes caused by synoptic scale advection. We also have this synoptic scale advection over the island but additionally the temperature changes are caused by the radiative heating or cooling of the underlying surface and other local effects. We therefore suppose that the temperature change with time on the lowest grid point is

$$\frac{\partial \Theta_1}{\partial t} + U \cdot \frac{\partial \Theta_1}{\partial x} = \frac{\partial \Theta_L}{\partial t} + \frac{\partial \Theta_S}{\partial t} \tag{77}$$

where

$\frac{\partial \Theta_S}{\partial t}$ is the temperature changes with time caused by synoptic advection,

$U \frac{\partial \Theta_1}{\partial x}$ is a local advection term and

$\frac{\partial \Theta_L}{\partial t}$ is the temperature changes with time caused by local effects.

Over the sea upstreams Gotland we have $\frac{\partial \Theta_1}{\partial t} = \frac{\partial \Theta_S}{\partial t}$ or $\Theta_1 = \Theta_S$ where Θ_S is given from the observed values at Stora Karlsö. To be able to determine $\frac{\partial \Theta_L}{\partial t}$ we are supposing that the local advection term, $U \frac{\partial \Theta}{\partial x}$, is much smaller than the $\frac{\partial \Theta_S}{\partial t}$ - term at the east coast of Gotland, which means $\Theta_L = \Theta_1 - \Theta_S$ where Θ_1 is the measured temperature at the east coast, here taken as the temperature at the synoptic station Herrvik, and Θ_S is the temperature at Stora Karlsö. Θ_S and Θ_L are plotted as functions of time in Fig 26.

As the temperature over Gotland is different from the temperature over the sea the pressure field over the island will be different from the pressure over the sea — a sea-breeze situation. This can be expressed as an additional geostrophic wind component over the island:

$$\left(U_{gt}, V_{gt}\right) = \frac{1}{\rho f}\left(-\frac{\partial P}{\partial y}, \frac{\partial P}{\partial x}\right) \tag{78}$$

As we have our x-axis perpendicular to the coast line we get only an additional geostrophic wind in the V_g-component. We obtain the pressure from the hydrostatic equation

$$\frac{\partial p}{\partial z} = -g \cdot \rho \tag{79}$$

by integrating over z. We express the density of the air, ρ, in terms of the potential temperature.

$$\rho = \left(p_0^{R/C_p} \cdot p^{C_v/C_p} \right) / R\Theta = p/RT \tag{80}$$

giving us

$$p(z) = \left\{ P_H^{R/C_p} + \frac{g}{C_p} p_0^{R/C_p} \int_z^H \frac{\partial z}{\Theta} \right\}^{C_p/R} \tag{81}$$

where

P_H is the pressure at the top of the model.
p_0 is the standard pressure at 2000 m (795 mbar).
R_L, C_p, C_v are constant.

The additional geostrophic wind component, V_{gt}, can now be determined from Eq (78) with the aid of Eq (80) and Eq (81).

Simulations have been performed between 0600 GMT and 1400 GMT for the several days The simulations have been compared with the measured wind-speeds. Figs 27-29 show some examples of the simulated wind fields over Gotland. In the figures measured 1 hour mean wind-speeds are also indicated at different heights above Näsudden, Eksta, Lojsta and När.

From these figures we can see that the model simulates the wind-speed decrease over the island fairly well. In table 5 the simulated and the measured differences between wind-speeds at Näsudden and at Lojsta are given for different heights. The differences obtained in the model are determined by the simulated wind profiles at 0900 GMT and at 1200 GMT. The measured differences are taken from the mean wind profiles obtained from all measurements before 1100 GMT and from all measurements in the afternoon, respectively.

Table 5. Differences between wind-speeds at Näsudden and at Lojsta at the levels 75 m, 125 m and 175 m. The reductions in percent of the wind-speed at Näsudden are given in brackets.

	75 m		125 m		175 m	
Date	Measured	Model	Measured	Model	Measured	Model
21/11 am	4.5 (36)	4.3 (36)	4.2 (34)	4.5 (38)	4.6 (33)	1.5 (11)
21/11 pm	7.0 (43)	3.8 (28)	5.5 (31)	3.6 (25)	4.0 (22)	3.2 (22)
22/11 am	3.9 (30)	2.5 (18)	5.0 (29)	2.4 (16)	5.1 (25)	3.3 (20)
22/11 pm	4.7 (33)	3.1 (20)	6.3 (37)	2.7 (17)	3.1 (18)	2.2 (13)
23/11 am	4.3 (35)	2.9 (20)	5.3 (37)	2.1 (14)	4.4 (30)	1.5 (10)
23/11 pm	3.5 (26)	2.9 (18)	3.7 (25)	2.3 (14)	2.5 (16)	1.6 (10)
Mean	4.7 (34)	3.3 (23)	5.0 (32)	2.9 (21)	4.0 (24)	2.2 (14)

We see from the table that the measurements give about 1.5 times larger reduction of the wind-speed at Lojsta than the simulations. A possible cause for these differences in the reduction of the wind-speed at Lojsta is the topography which is not included in the model. Näsudden is situated at about sea level and Lojsta at about 80 m above sea level. Another possible cause is that we might have simulated a wrong temperature stratification over the island as we give the measured temperature profile at Visby 1200 GMT as an initial profile at 0600 GMT in the simulations. Furthermore it is important to point out that we are trying to simulate a three-dimensional world with a two-dimensional model which can induce considerably faults.

The differences between wind-speeds at Näsudden and När are given in Table 6. We see from the table that the agreement as a mean over the whole measurement campaign is very good but there are large differences between the individual days.

In view of the fact that the experiment situation was far from ideally two-dimensional the simulations of the Gotland data show fairly good agreement.

Table 6. Differences between wind-speeds at Näsudden and at När at the levels 75 m, 125 m and 175 m. The reductions in percent of the wind-speed at Näsudden are given in brackets.

	75 m		125 m		175 m	
Date	Measured	Model	Measured	Model	Measured	Model
21/11 am	3.6 (30)	3.4 (29)	1.7 (14)	3.6 (28)	2.7 (19)	3.2 (24)
21/11 pm	3.9 (24)	3.8 (30)	3.6 (20)	3.9 (28)	3.2 (17)	4.2 (29)
22/11 am	0.6 (4)	2.6 (18)	0.9 (5)	3.3 (23)	1.0 (4)	4.6 (27)
22/11 pm	5.0 (34)	3.1 (20)	5.2 (31)	3.1 (19)	3.8 (22)	3.0 (18)
23/11 am	0.6 (5)	3.1 (22)	1.0 (7)	2.6 (17)	-0.4 (-3)	2.2 (14)
23/11 pm	3.2 (23)	2.5 (16)	3.4 (24)	2.3 (14)	2.8 (17)	2.0 (12)
Mean	2.8 (20)	3.1 (23)	2.8 (17)	2.4 (22)	1.8 (13)	2.5 (21)

SUMMARY AND CONCLUSIONS

A two-dimensional second-order closure model is presented. The model requires solutions of differential equations for mean wind and temperature and of two partial differential equations for the total turbulent kinetic energy and the temperature variance respectively. The remaining second-order moments are solved by using a set of algebraic equations. The simulations incorporate observed values for the geostrophic winds, the thermal winds and the temperature at screen height. For the turbulent length scale Yamada and Mellor (1975) make a very simple approach. In the present model available experimental atmospheric data as well as laboratory data have been used to define a much more sophisticated formulation for these scales. The equation for the conservation of the mean mixing ratio of water vapor is not included in the set of equations, limiting us to look at situations where no boundary layer clouds or fog exist.

The one-dimensional version of the model is tested against the Wangara data DAY33 through DAY35 (Clarke et al., 1971). The computed wind and potential temperature agree qualitatively and quantitatively with the observed values. However, during the night we get a too shallow surface inversion layer which is probably caused by the fact that we have excluded the radiative term in the temperature equations. It is also shown that the wind profiles during the nights agree much better with the measured ones if the velocity advection terms are included in the mean wind equations.

The convective boundary layer height is shown to agree excellently with the measured height during DAY33. Also during DAY34 the agreement is very good, but the growth of the convective layer preceeds a little bit too slow during the first hour. The present model shows a much better agreement with the measured height than Yamada's and Mellor's one-dimensional model, which the present model is based upon.

The turbulent quantities are compared with other models, atmospheric measurements and laboratory experiments. To be able to compare the results with atmospheric measurements at other sites and with laboratory experiments the turbulent quantities have to be normalized. Deardorff (1970) has shown that a scaling based on the convective velocity w_*, temperature $T_* = Q_0/w_*$ and the height of the mixed layer z_i produces universal profiles of the turbulent quantities in a dry convective boundary layer. The results from the present model have therefore been presented in a dimensionless form.

The vertical profiles of the dimensionless velocity variance are similar in shape to data both from field measurements and from laboratory experiments. In the lowest part of the convective boundary layer the model, however, seems to transfer too much of the turbulent energy into the vertical component. This is also evident in the profiles of the horizontal components of the turbulent energy for which Deardorff's 3-D model predicts a decrease with height in the lowest part of the atmosphere. The present model predicts a constant value up to 0.8 z_i, above that height a decrease of the horizontal turbulent energy is predicted.

The temperature variance profiles, made dimensionless by T_*^2, are very similar to the results from other models and experiments, showing that the scaling with T_* and z_i produce universal profiles of the temperature variance up to about 0.8 z_i in the convective boundary layer.

The heat flux has been made dimensionless by its surface value. It decreases nearly linearly with height in the convective layer, as observed in nature and in laboratory experiment. The magnitude of the negative kinematic heat flux in the stable layer above the convective layer is about the same as that obtained in the experiments and Deardorff's 3-D model.

The results obtained in the one-dimensional version of the present model show that it can predict mean quantities and turbulent quantities almost as good as much more complicated models if proper proportionality factors for the mixing length scales are used. This type of model is also much less computer time consuming as it solves only two out of ten differential equations for the second order moments and it can therefore be more easily used in applied studies.

In the test of the two-dimensional version of the model we have only been able to compare the mean wind components against field measurements. Those measurements were performed in the island of Gotland (Faxén, 1980). Unfortunately the experimental situation was far from ideally two-dimensional. In spite of this the model shows a fairly good agreement with several of the Gotland measurements.

ACKNOWLEDGEMENTS

This work has been carried out in partial fulfilment of the degree of Doctor of Philosophy. It has been sponsored by the Swedish Military Weather Service and the National Swedish Environment Protection Board (SNV 7-306178). The Gotland experiment and some analysis effort has been sponsored by the Swedish National Board for Energy Source Development under contract nr 5060100.

I wish to thank the many colleagues and members of the technical staff at the Department of Meteorology, Uppsala, who have been very helpful during the various stages of this work. I will especially express my sincere thanks to my supervisor Professor Ulf Högström and to my colleague Hans Bergström for fruitful discussions and advice.

REFERENCES

André, J.C., G. de Moor., P. Lacarrère and R. du Vachat, 1976: *Turbulence approximation for inhomogeneous flows: Part II. The numerical simulation of a penetrative convection experiment.* J. Atm. Sci., 33, 482-491.

André, J.C., G. de Moor., P. Lacarrère, G. Therry and R. du Vachat, 1978: *Modeling the 24-hour evolution of the mean and turbulent structures of the planetary boundary layer.* J. Atmos. Sci., 35, 1861-1883.

Blackadar, A.K, 1962: *The vertical distribution of wind and turbulent exchange in neutral atmosphere.* J. Geophy. Res., 67, 3095-3102.

Caughey, S.J. and S.G. Palmer, 1979: *Some aspects of turbulence structure through the depth of the convective boundary layer.* Quart. S. Roy. Meteor. Soc., 105, 811-827.

Caughey, S.J, 1982: *Observed characteristics of the atmospheric boundary layer,* in: Atmospheric turbulence and air pollution modelling, F.T.M. Nieuwstadt and H. van Dop, Editors. D. Reidel Publishing Company, Dodrecht, Holland, 107-158.

Clarke, R.H., R.R. Brook., D.G. Reid and A.J. Troup, 1971: *The Wangara experiment: Boundary layer data.* Tech. Paper. 19. Div. Meteor. Phys., CSIRO, Australia.

Deardorff, J.W, 1970: *Convective velocity and temperature scales for the unstable planetary boundary layer and for Rayleigh convection.* J. Atmos. Sci., 27, 1211-1213.

Deardorff, S.W, 1974: *Three-dimensional numerical study of turbulence in an entraining mixed layer.* Boundary-Layer Meteorol., 7, 199-226.

Delage, Y, 1974: *A numerical study of the nocturnal atmospheric boundary layer.* Quart. J. Roy. Meteor. Soc., 100, p. 351.

Estoque, M.A, 1963: *A numerical model of the atmospheric boundary layer.* J. Geophys. Res., 68, 1103-1113.

Faxén, T, 1980: *The Gotland-Skåne pibal project for wecs siting. Part A: Measurements.* Department of Meteorology, University of Uppsala, Sweden, Reports No 62.

Grandin, G, 1983: *A one-dimensional PBL model with a subgrid-scale condensation scheme for stratiform clouds and fog*. Department of Meteorology, University of Uppsala, Sweden. Reports No 72.

Haugen, D.A., J.C. Kaimal and E.F. Bradley, 1971: *An experimental study of Reynolds stress and heat flux in the atmospheric surface layer*. Quart. J. Roy. Meteor. Soc., 97, 168-180.

Högström, U., R. Taesler., S. Karlsson., L. Enger and A.S. Smedman-Högström, 1978: *The Uppsala urban meteorology project*. Boundary-Layer Meteor., 15, 69-80.

Izumi, Y. and S.J. Caughey, 1976: *Minnesota 1973 atmospheric boundary layer experiment data report*. AFGL Environmental Research Paper, no 547.

Kaimal, J.C., J.C. Wyngaard., P.A. Haugen., O.R. Cotē, Y. Izumi., S.J. Caughey and C.J. Readings, 1976: *Turbulent structure in the convective boundary layer*. J. Atmos. Sci., 33, 2152-2169.

Lewellen, W.S. and M. Teske, 1975: *Turbulence Modeling and its application to atmospheric diffusion. Part II. Critical review of the use of invariant modeling*. EPA-600/4-75-016b, December 1975. 50 pp.

Mellor, G. and H.J. Herring, 1973: *A survey of mean turbulent field closure models*. AIAA J., 11, 590-599.

Mellor, G. and T. Yamada, 1974: *A hierarchy of turbulence closure models for planetary boundary layer*. J. Atmos. Sci., 31, 1791-1806.

Monin, A.S. and A.M. Yaglom, 1977: *Statistical fluid mechanics: Mechanics of turbulence*. Vol 1, J.L. Lumley, Ed. The MIT Press, Cambridge, Mass, 769 pp.

Panofsky, H.A., H. Tennekes., D.H. Lenshow and J.C. Wyngaard, 1977: *The characteristics of turbulent velocity components in the surface layer under convection conditions*. Boundary-Layer Meteor., 11, 355-361.

Paulsson, C.A, 1970: *The mathematical representation of wind speed and temperature profiles in the unstable atmospheric surface layer*. J. Appl. Meteor., 9, 857-861.

Richtmyer, R.D. and K.W. Morton, 1967: *Difference methods for initial-value problems*. Interscience 405 pp.

Tennekes, H. and J.L. Lumley, 1972: *A first course in turbulence*. MIT Press, Cambridge, Mass. 300 pp.

Tennekes, H, 1982: *Similarity relation, scaling laws and spectral dynamics*, in: Atmospheric turbulence and air pollution modelling, F.T.M. Nieuwstadt and H. van Dop, Eds. D. Reidel Publishing Company, Dordrecht, Holland, 37-68.

Willis, G.E. and S.W. Deardorff, 1974: *A laboratory model of the unstable planetary boundary layer.* J. Atm. Sci., 31, 1297-1307.

Wyngaard, S.C. and O.R. Coté, 1971: *The budgets of turbulent kinetic energy and temperature variance in the atmospheric surface layer.* J. Atmos. Sci., 28, 190-201.

Wyngaard, J.C., O.R. Coté and Y. Izumi, 1971: *Local free convection, similarity, and the budgets of shear stress and heat flux.* J. Atm. Sci., 28, 1171-1182.

Wyngaard, J.C. and O.R. Coté, 1974: *The evolution of a convective planetary layer – a higher-order-closure model study.* Boundary-Layer Meteorol., 7, 284-308.

Yamada, T. and G. Mellor, 1975: *A simulation of the Wangara atmospheric boundary layer data.* J. Atmos. Sci., 32, 2309-2329.

Yamada, T, 1979: *An application of a three-dimensional, simplified second-moment closure numerical model to study atmospheric effects of a large cooling-pond.* Atmos. Environment, 13, 693-704.

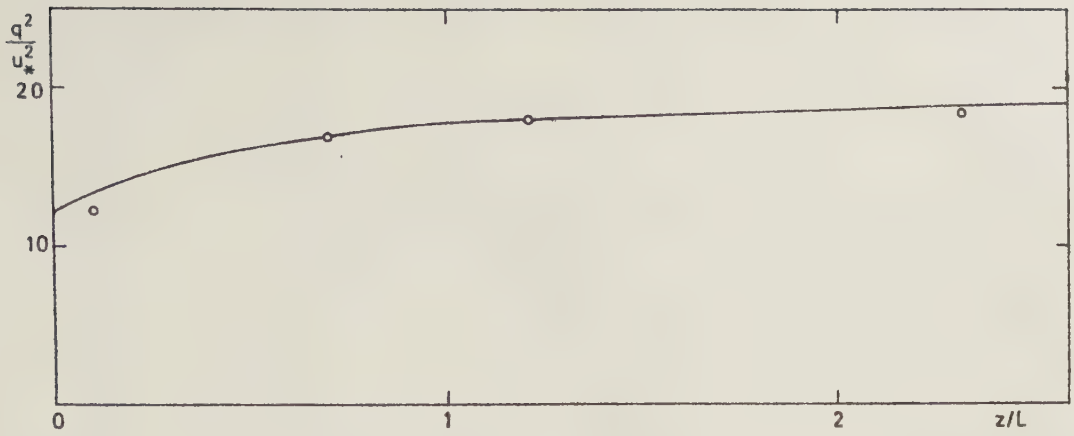

Fig 1. The normalized turbulent energy q^2/u_*^2, as a function of the stability parameter z/L. The full line represents the relationship Eq (25). The rings are mean values of q^2/u_*^2 from the turbulent measurements at the Gränby site, Uppsala and at the islet Näskär in the archipelago of Stockholm for different stability classes.

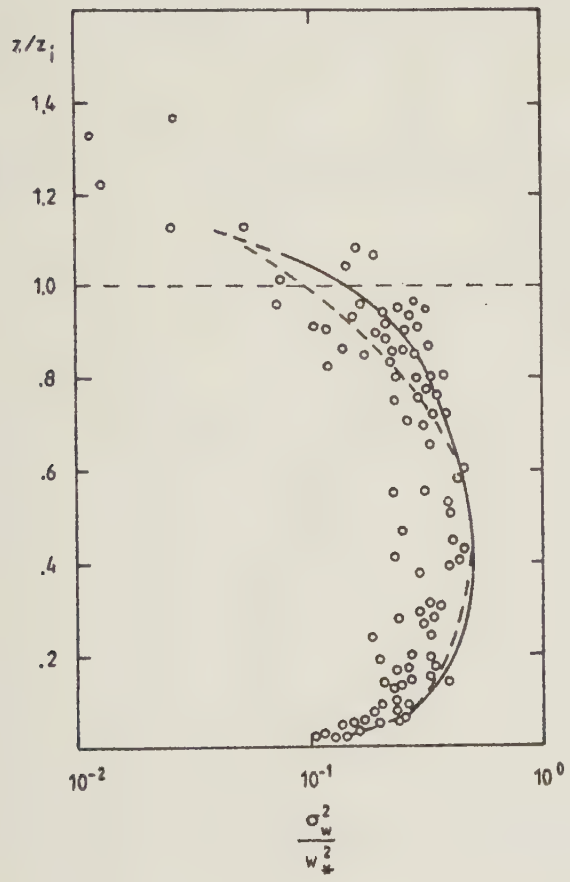

Fig 2. Normalized vertical variance. Rings are the Ashchurch (Caughey and Palmer, 1979) and the Minnesota data (Izumi and Caughey, 1976). The dashed line represents the results from Willis' and Deardorff's (1974) tank experiment. The full line represents the relationship Eq (40a).

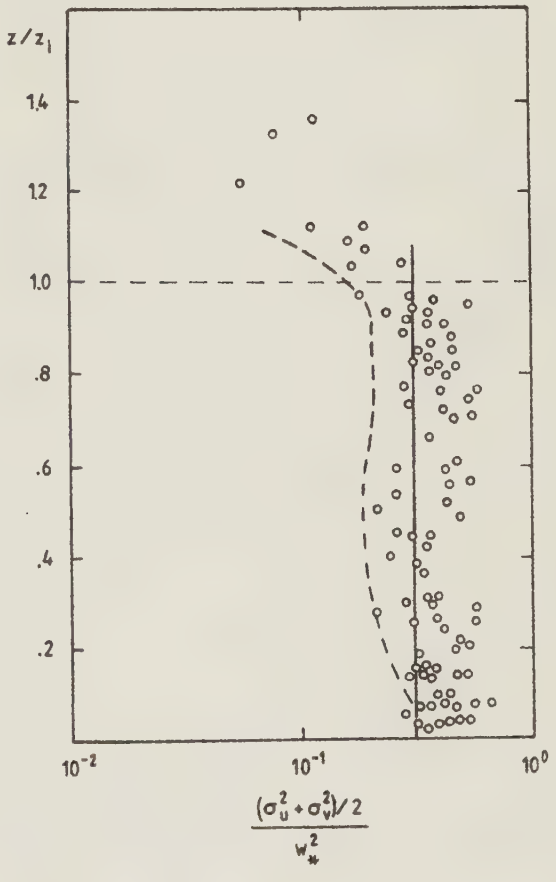

Fig 3. The average of the normalized horizontal velocity components. Rings and dashed line coded as in Fig 2. The full line represents Eq (41).

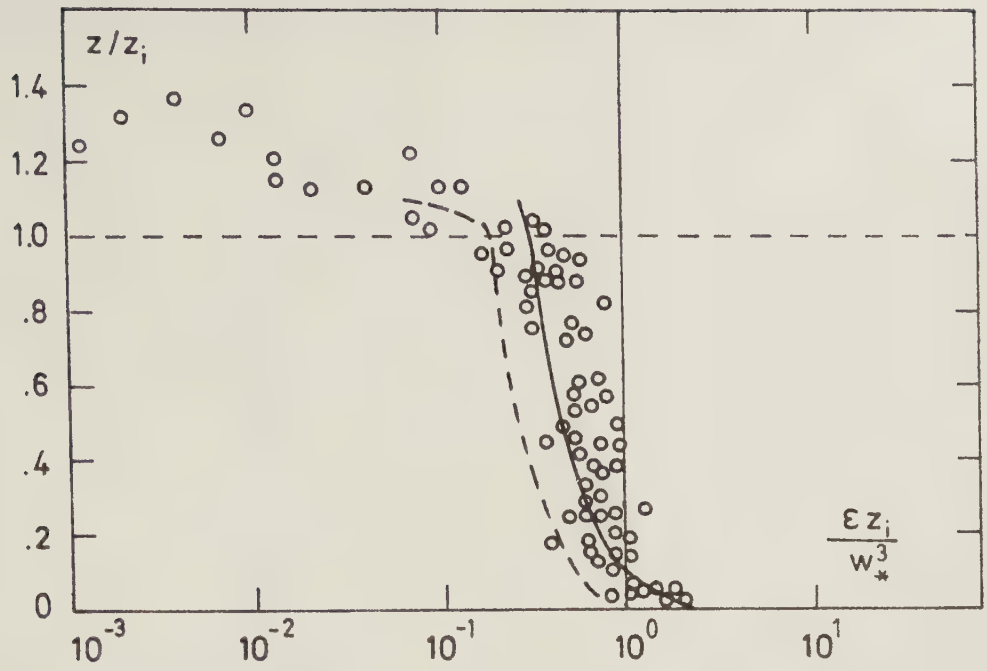

Fig 4. Variation of the normalized dissipation rate of turbulence kinetic energy with height. Rings and dashed line coded as in Fig 2. The full line represents Eq (43).

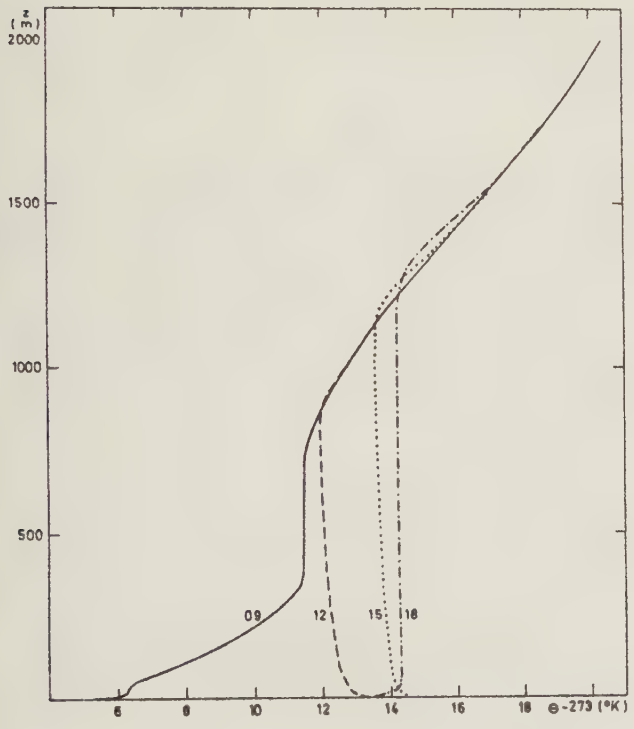

Fig 5a. Computed profiles of the mean potential temperature at various times on DAY33.

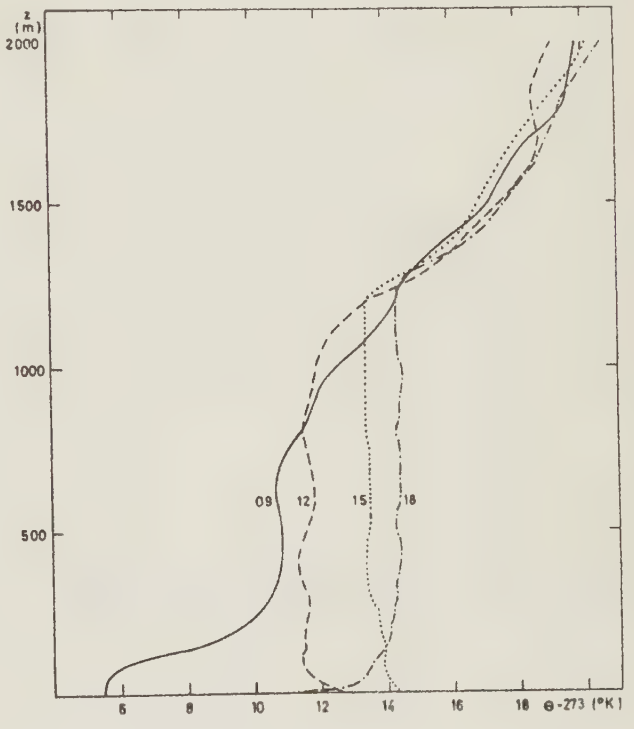

Fig 5b. Observed profiles of the mean potential temperature at various times on DAY33.

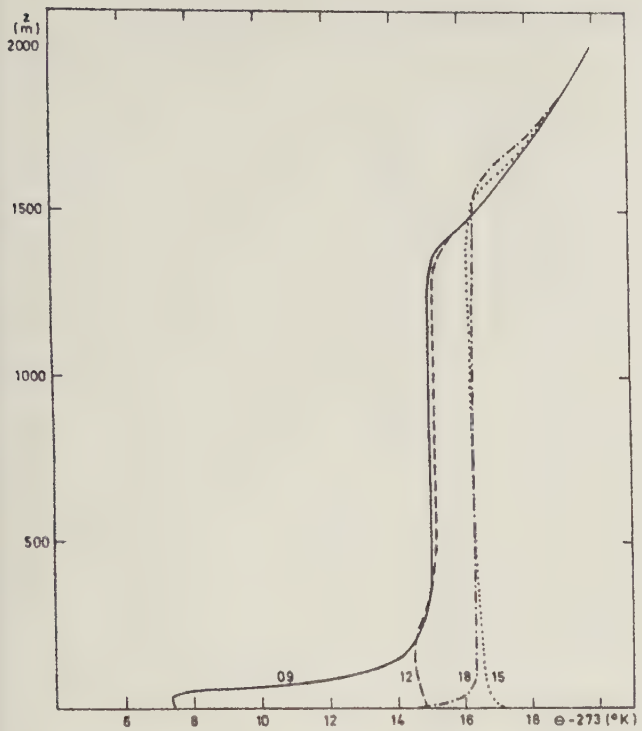

Fig 6a. Computed profiles of the mean potential temperature at various times on DAY34.

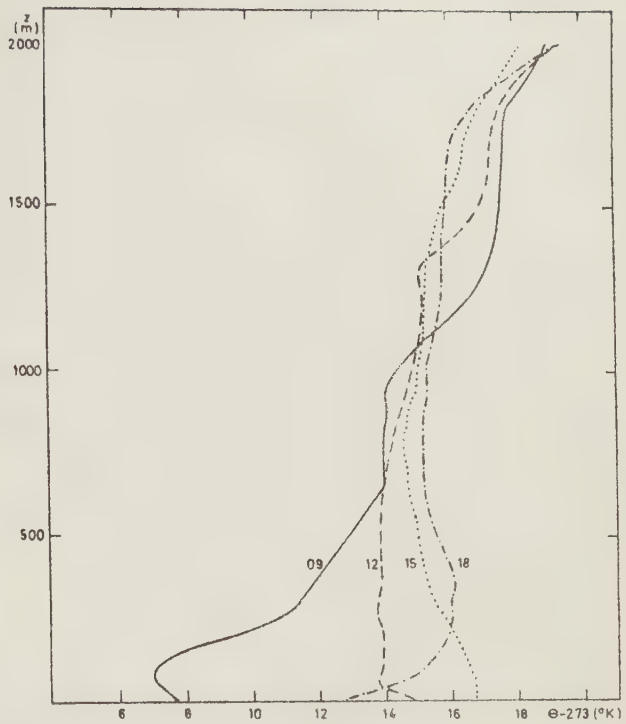

Fig 6b. Observed profiles of the mean potential temperature at various times on DAY34.

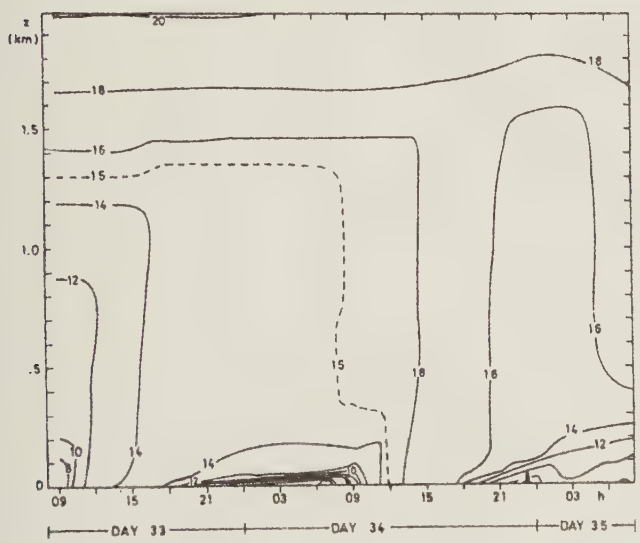

Fig 7a. Time and space variation of the computed mean potential temperature. The values on the contour lines (θ-273) are in units of degrees K.

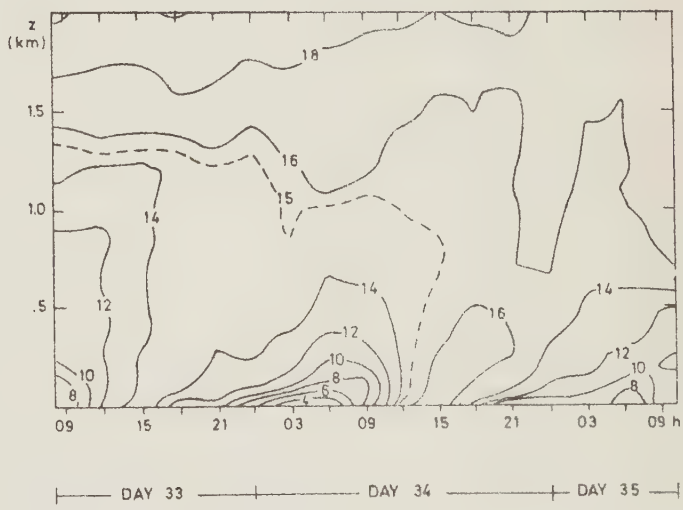

Fig 7b. Time and space variation of the observed mean potential temperature. The values on the contour lines (θ-273) are in units of degrees K.

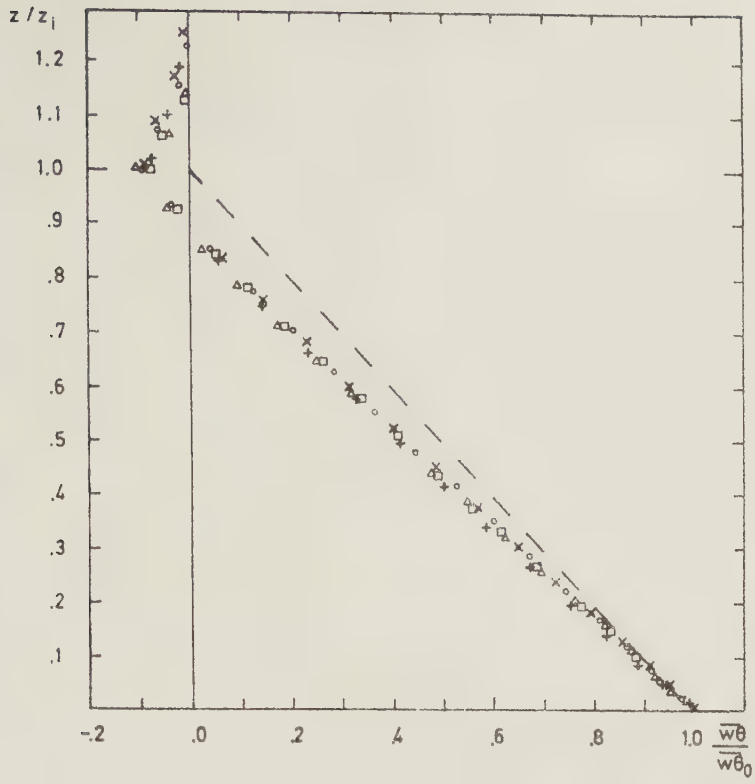

Fig 8. Normalized heat flux at various times on DAY33.
+ = 12.00, x = 13.00, o = 14.00, Δ = 15.00, □ = 16.00.

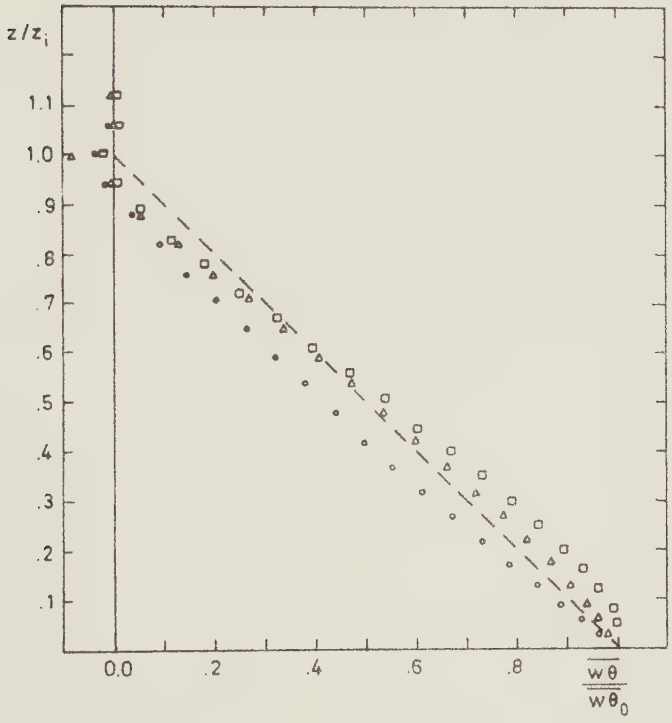

Fig 9. Normalized heat flux at various times on DAY34.
Symbols as in Fig 8.

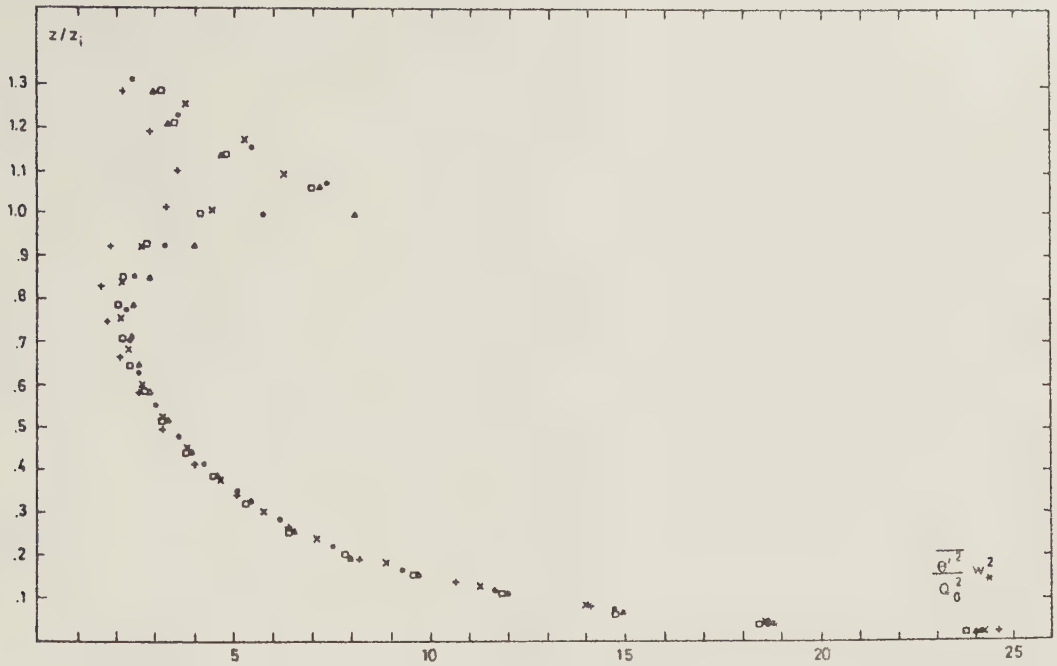

Fig 10. Normalized temperature variance at various times on DAY33. Symbols as in Fig 8.

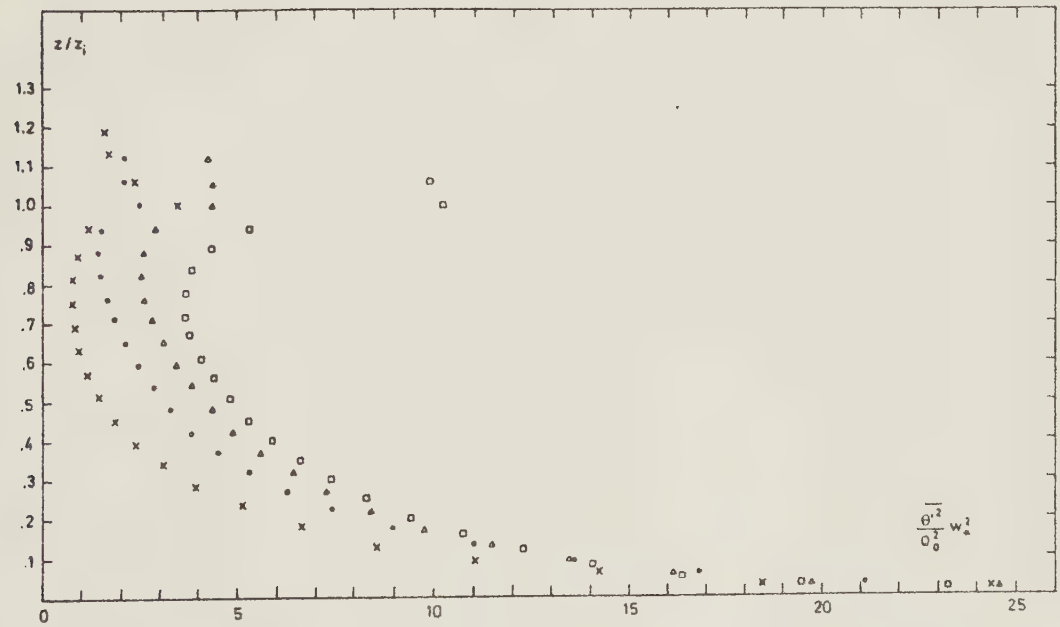

Fig 11. Normalized temperature variance at various times on DAY34. Symbols as in Fig 8.

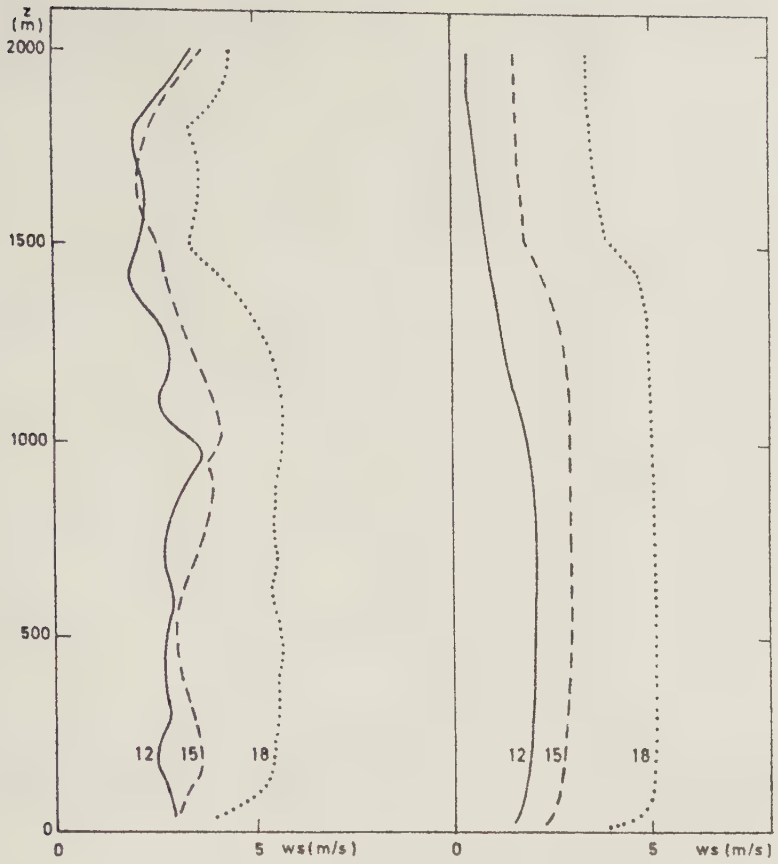

Fig 12. Observed (left) and computed (right) wind-speed profiles at various times on DAY33.

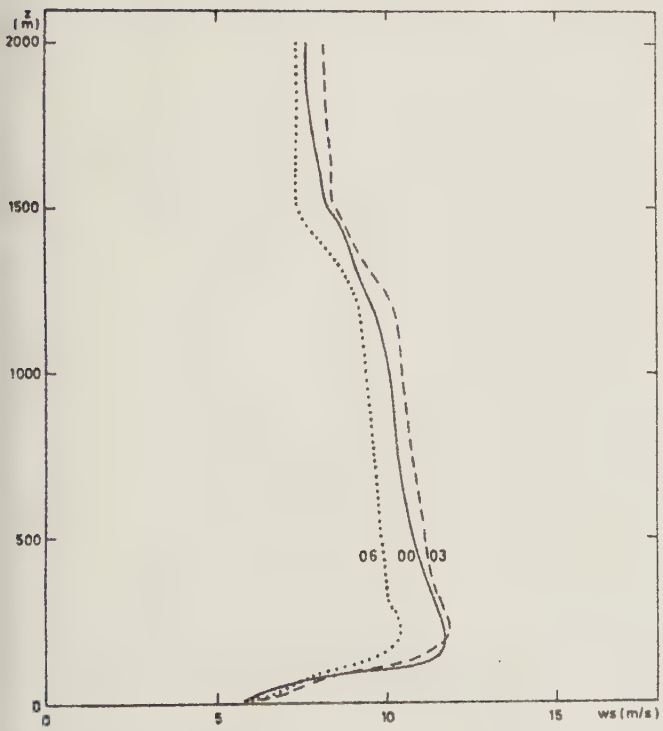

Fig 13a. Computed wind-speed profiles at various times on DAY34.

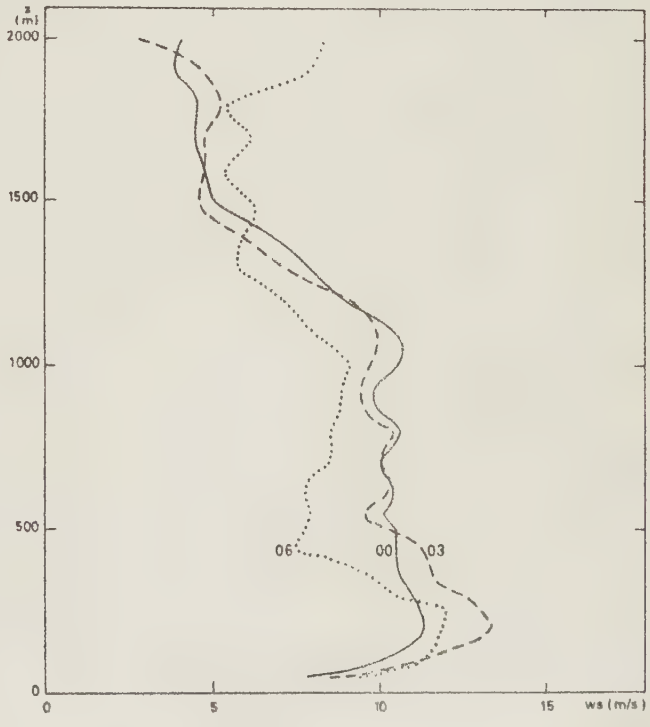

Fig 13b. Observed wind-speed profiles at various times on DAY34.

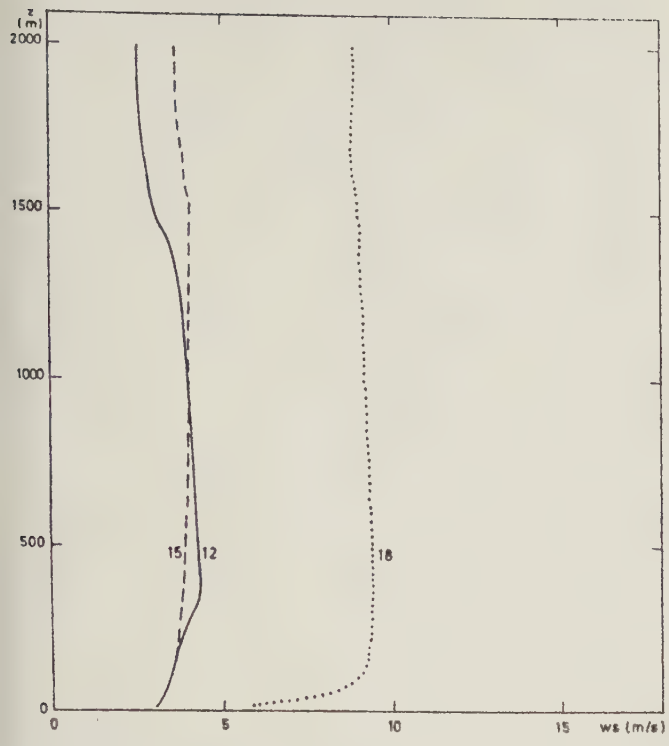

Fig 14a. Computed wind-speed profiles at various times on DAY34.

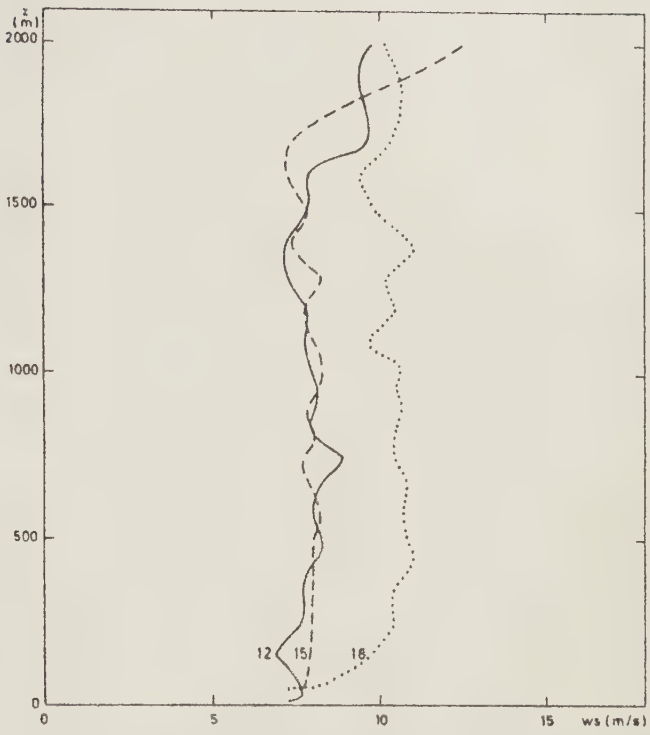

Fig 14b. Observed wind-speed profiles at various times on DAY34.

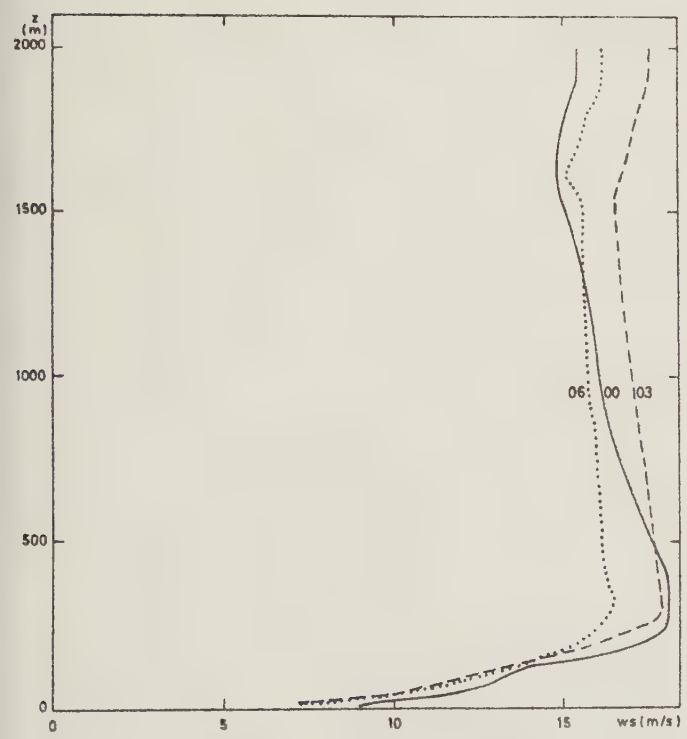

Fig 15a. Computed wind-speed profiles at various times on DAY35.

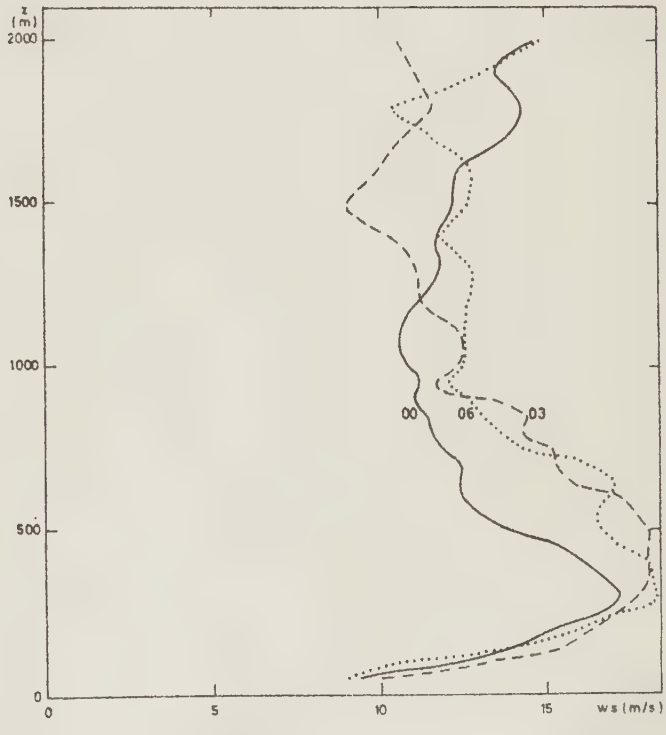

Fig 15b. Observed wind-speed profiles at various times on DAY35.

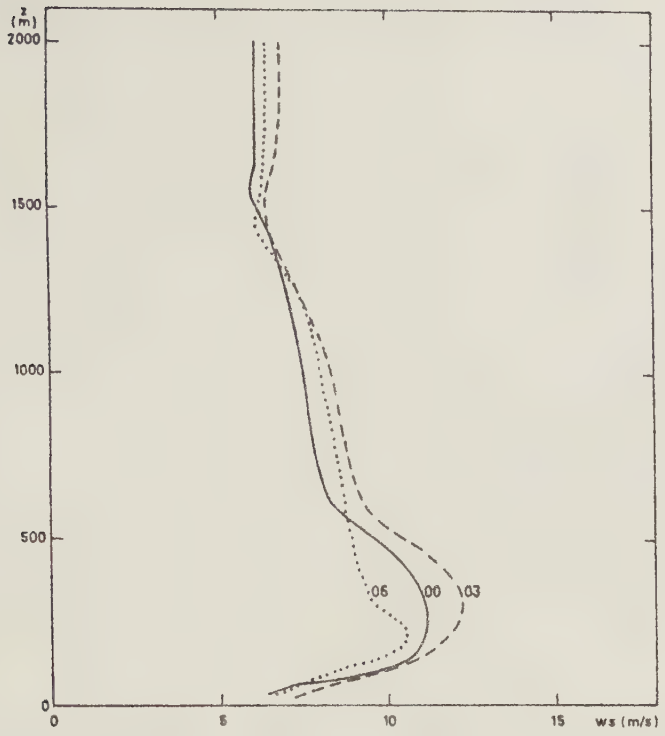

Fig 16. Computed wind-speed profiles at various times on DAY34 with a 'synoptic advection term' included in the wind equations (see text).

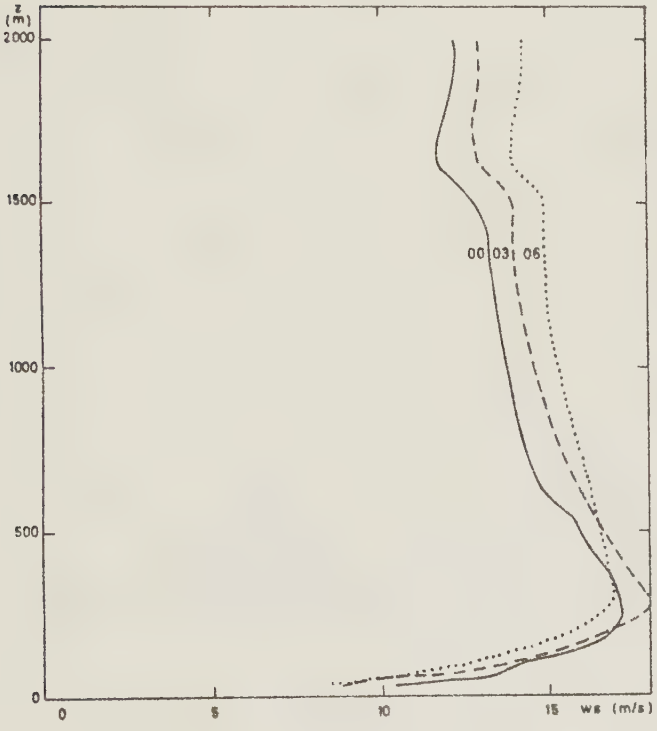

Fig 17. Computed wind-speed profiles at various times on DAY35 with a 'synoptic advection term' included in the wind equations (see text).

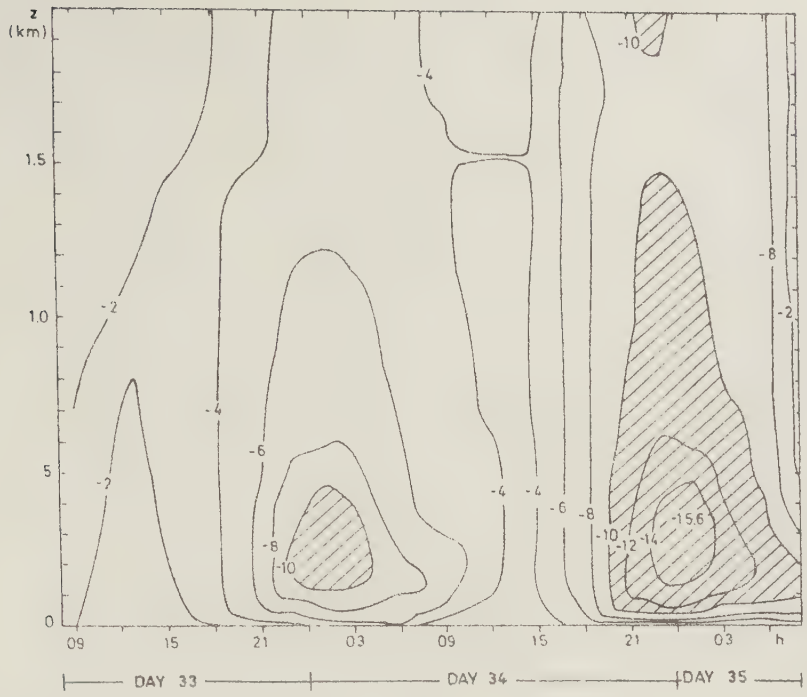

Fig 18a. Time and space variation of the computed eastward mean wind component U. The synoptic advection terms are included in the equations (see text). The values on the contour lines are in units of meters per second.

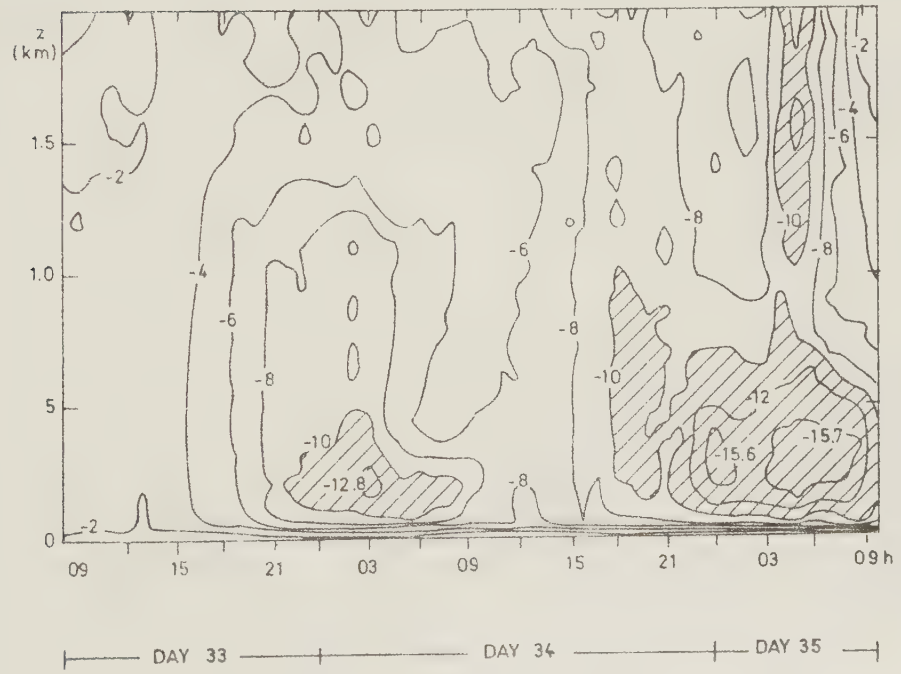

Fig 18b. Time and space variation of the observed eastward mean wind component.

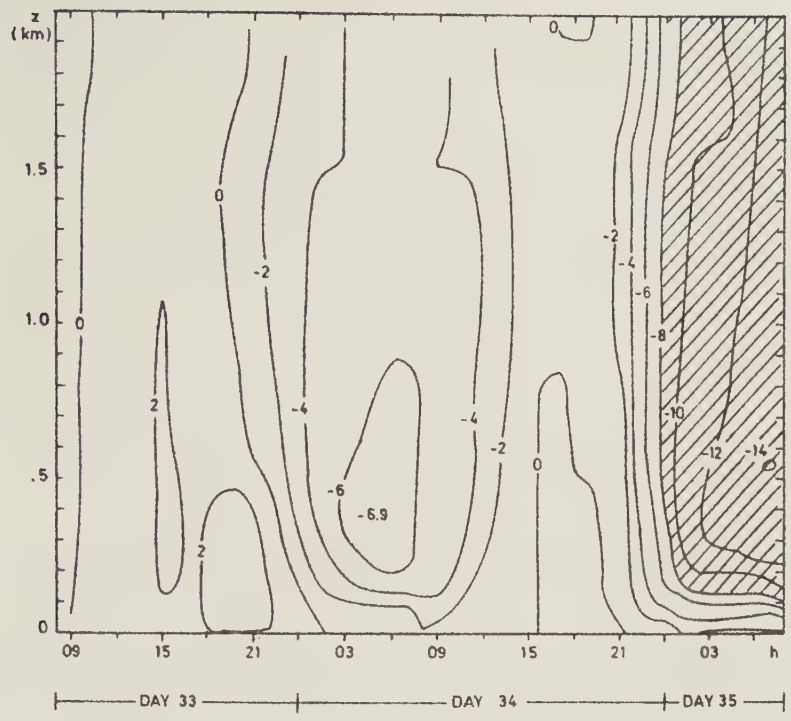

Fig 19a. As in Fig 18a except for the northward mean wind component V.

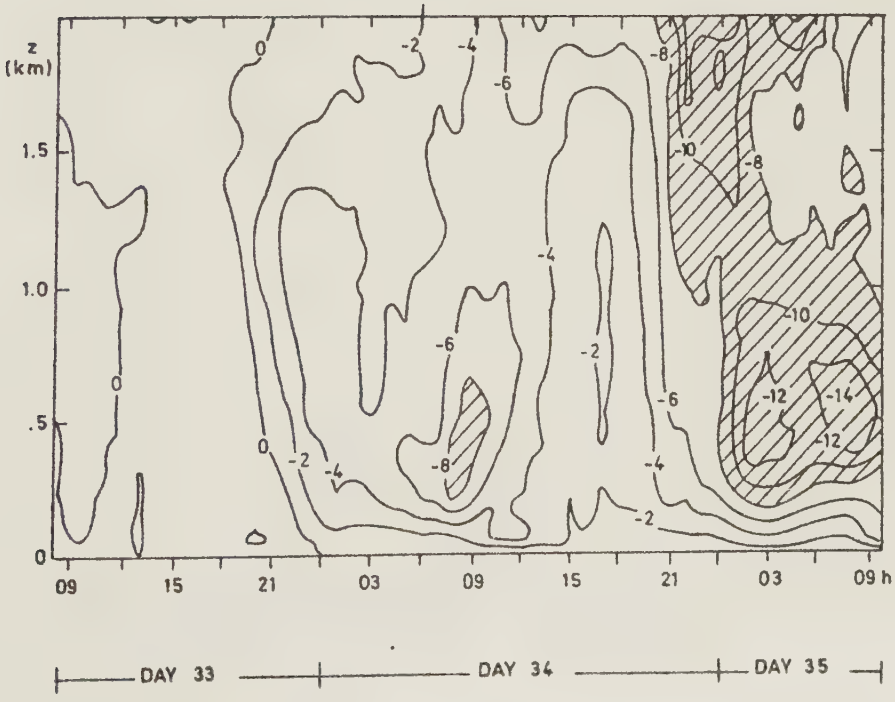

Fig 19b. As in Fig 18b except for the northward mean wind component.

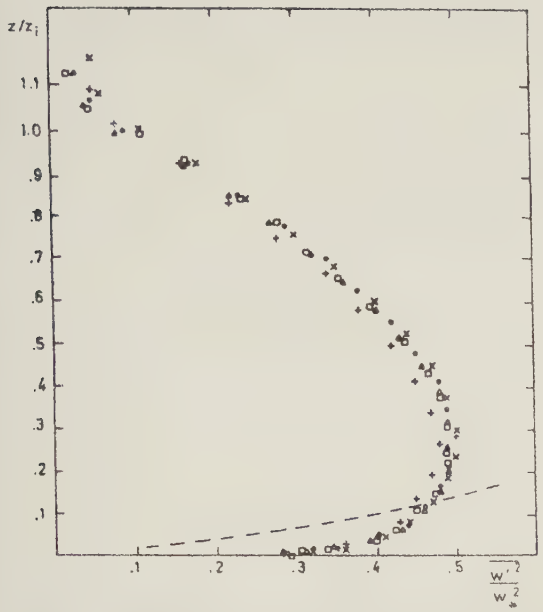

Fig 20. Computed normalized vertical variance at various times on DAY33. Symbols as in Fig 8.

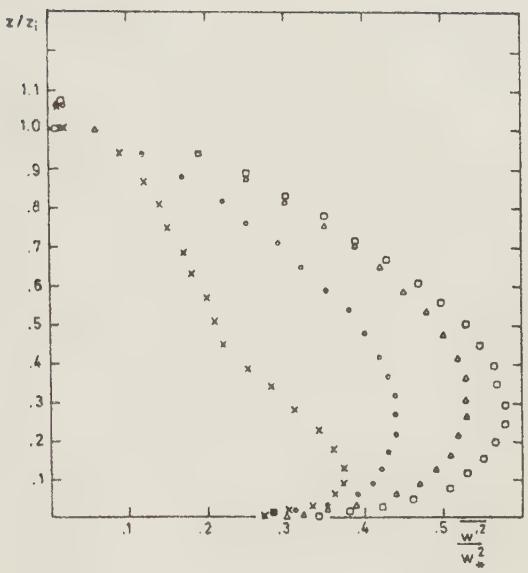

Fig 21. Computed normalized vertical variance at various times on DAY34. Symbols as in Fig 8.

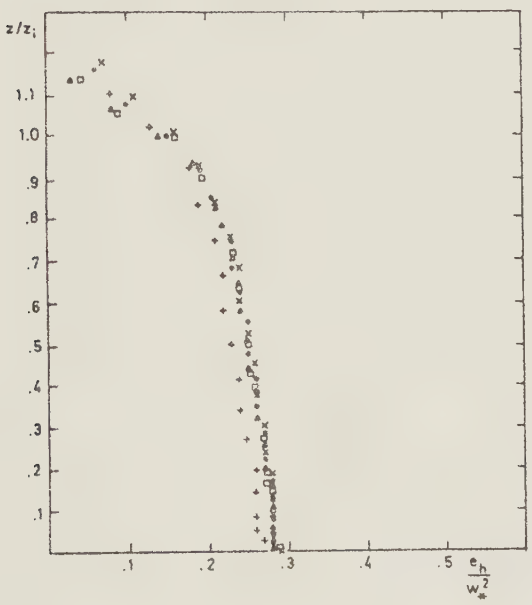

Fig 22. Computed normalized horizontal variance at various times on DAY33. Symbols as in Fig 8.

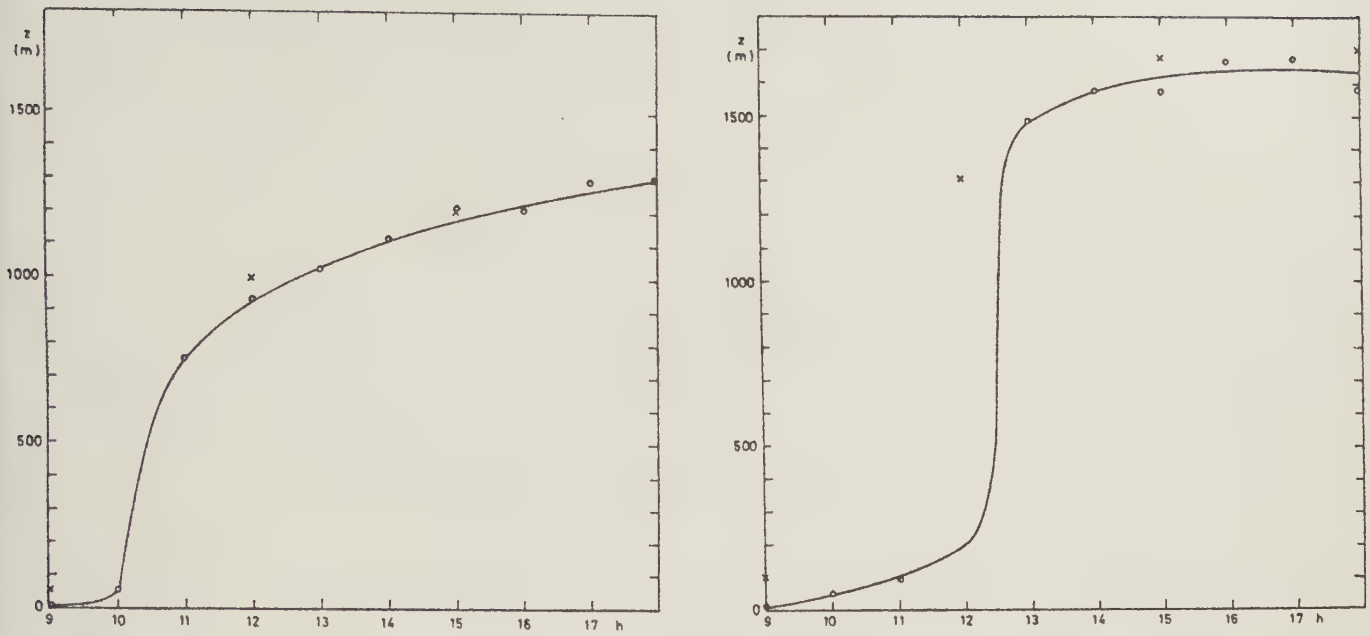

Fig 23. Time evolution of computed (o) and observed (x) mixing layer height on DAY33 (left) and DAY34 (right).

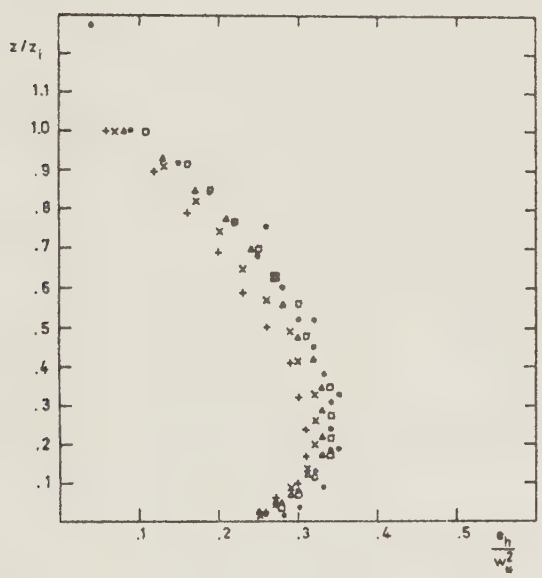

Fig 24. Computed normalized horizontal variance at various times on DAY33. Computed with the diffusion coefficients $a_1 = a_2 = 0.23$ (see text). Symbols as in Fig 8.

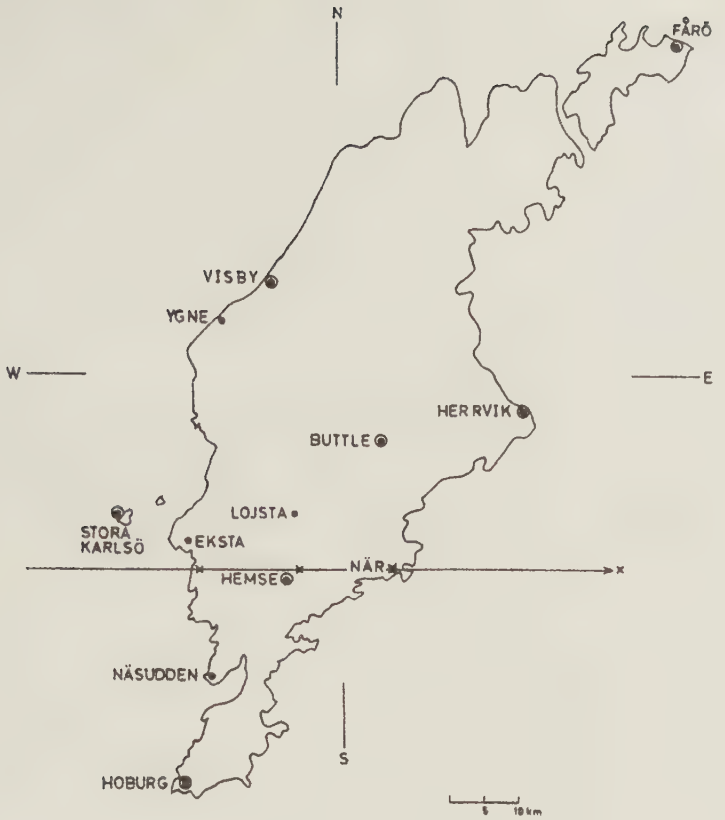

Fig 25. Map of Gotland showing the location of the pibal measurement sites and synoptical weather stations. The crosses (x) show the projected measurement sites on the x-axis (see text).

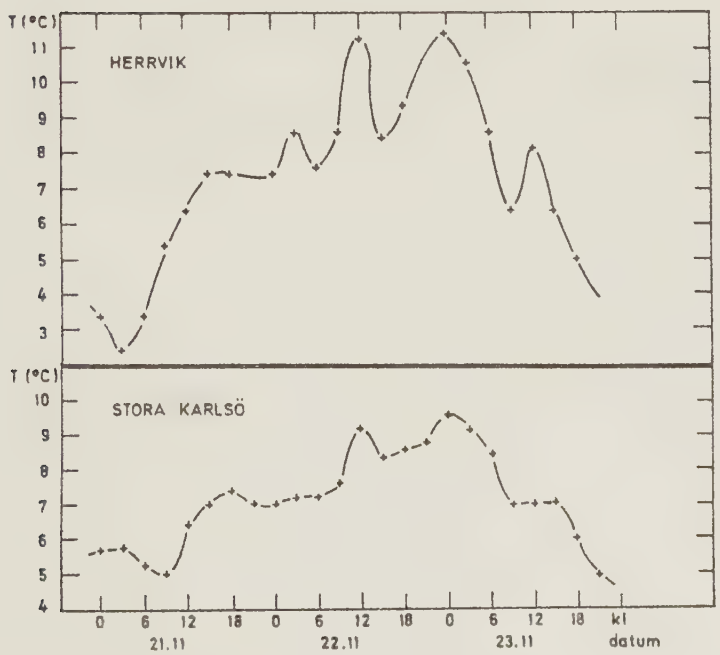

Fig 26. Time variation of the observed temperature at screen height at the synoptic stations Stora Karlsö and Herrvik.

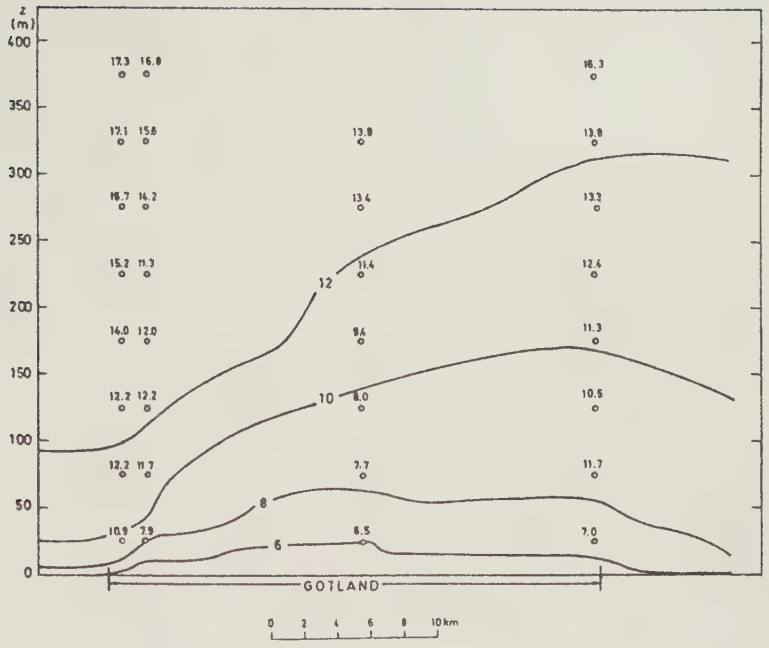

Fig 27. Space variation of the computed mean wind-speed over Gotland, 21 November 1978 at 1000 GMT. Circles with figures are measured mean wind-speeds. The figures are in units of meters per second.

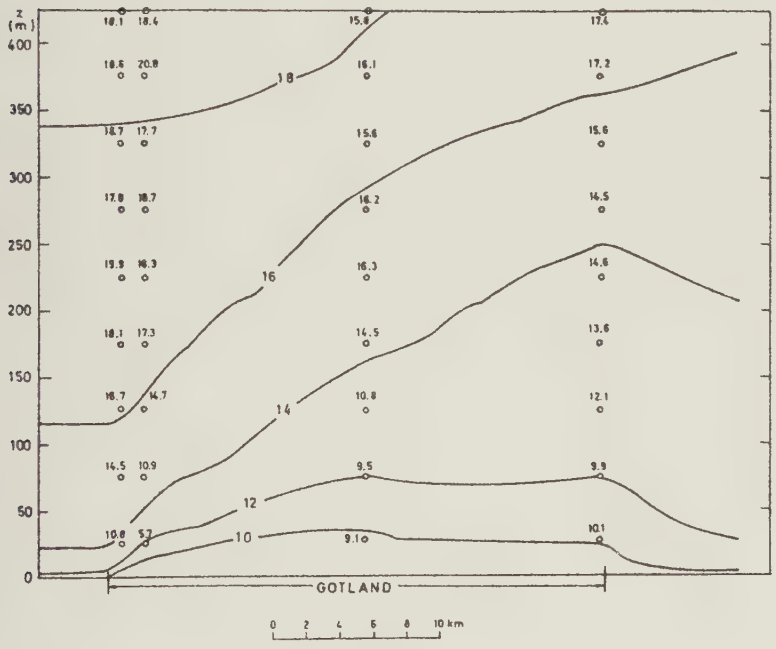

Fig 28. As Fig 27 except for 22 November 1978 at 1300 GMT.

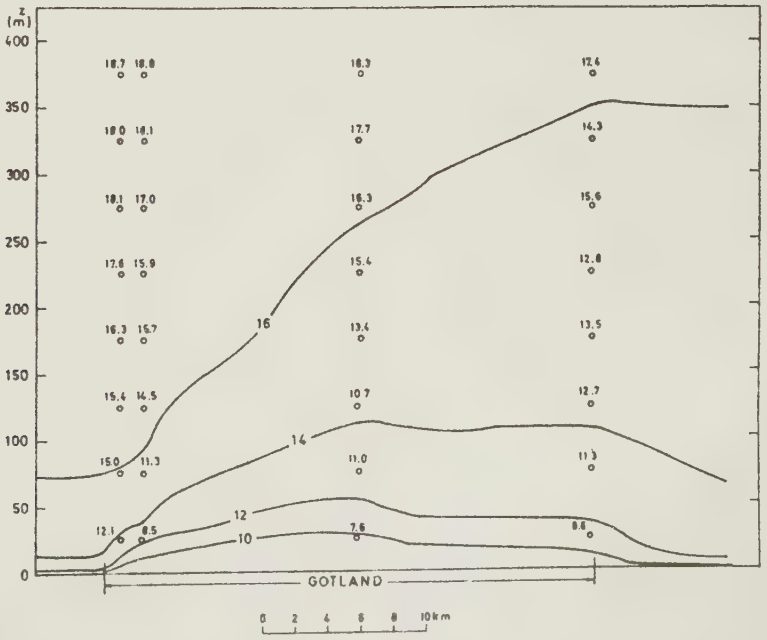

Fig 29. As Fig 27 except for 23 November 1978 at 1300 GMT.

Distributed by
Department of Meteorology
Uppsala University
Uppsala, SWEDEN

ISBN 91-506-0385-X